INSTITUT DE FRANCE
Académie des sciences

Comptes Rendus

Géoscience

Sciences de la Planète

Damir Slovenec, Mirko Belak, Luka Badurina, Marija Horvat and Branimir Šegvić

Triassic evolution of the Adriatic-Dinaridic platform's continental margins—insights from rare dolerite subvolcanic intrusions in External Dinarides, Croatia

Volume 355 (2023), p. 35-62

Published online: 12 January 2023

https://doi.org/10.5802/crgeos.183

Les Comptes Rendus. Géoscience — Sciences de la Planète *sont membres du Centre Mersenne pour l'édition scientifique ouverte*
www.centre-mersenne.org
e-ISSN : 1778-7025

Comptes Rendus
Géoscience — Sciences de la Planète
2023, Vol. 355, p. 35-62
https://doi.org/10.5802/crgeos.183

Original Article — Petrology, Sedimentology

Triassic evolution of the Adriatic-Dinaridic platform's continental margins—insights from rare dolerite subvolcanic intrusions in External Dinarides, Croatia

Évolution triasique des marges continentales de la plateforme Adriatique-Dinaridique — aperçu de l'étude des rares intrusions subvolcaniques de dolérite dans les Dinarides externes de Croatie

Damir Slovenec [a], **Mirko Belak** [a], **Luka Badurina** [b], **Marija Horvat** [a] **and Branimir Šegvić** [*, b]

[a] Croatian Geological Survey, Sachsova 2, 10000 Zagreb, Croatia

[b] Department of Geosciences, Texas Tech University, 1200 Memorial Circle, Lubbock, TX 79409, USA

E-mails: damir.slovenec@hgi-cgs.hr (D. Slovenec), mbelak@hgi-cgs.hr (M. Belak), luka.badurina@ttu.edu (L. Badurina), mhorvat@hgi-cgs.hr (M. Horvat), branimir.segvic@ttu.edu (B. Šegvić)

Abstract. This contribution reports new findings on petrogenesis and possible geotectonic setting of rare subvolcanic Triassic(?) dolerite cropping out in External Dinarides with a goal to contribute to the debate on the geodynamic evolution of the continental margin of the Adriatic-Dinaridic platform(s) at the onset of the Mesozoic. Petrography of the studied rocks revealed the crystallization order: clinopyroxene → plagioclase → alkali-feldspar ± amphibole ± Fe–Ti oxides. The geochemistry of calc-alkaline dolerite suggested magma generation from a spinel–garnet bearing peridotite mantle source (60sp:40grt). Two mechanisms explaining the origin of dolerite are here suggested. The first one involves a low-grade partial melting of the altered lithospheric mantle and the subduction-modified oceanic lithosphere accompanied with subducted/recycled sediments. The second one proposes a melting of the subduction-altered heterogeneous lithospheric (subcontinental) mantle contaminated and/or metasomatized during an earlier Variscan subduction in the Late Paleozoic. Accordingly, two geodynamic interpretations are suggested: (i) Middle Triassic north-vergent active subduction of the Paleotethys beneath the Andean-type active Laurasian continental margin coupled by the formation of a pericontinental volcanic arc and subsequent extension and back-arc rifting, within the Adria Plate, which led to the formation of locally aborted rift systems and subsidence of the platform, and (ii) Middle Triassic extension, unaffected by contemporaneous active subduction, of the High Karst

* Corresponding author.

nappe unit of the Greater Adria as a result of an ephemeral syn-rift volcanic stage, which featured the formation of the Dinaridic aborted rift system followed by the platform subsidence and emergence of local sedimentary basins.

Résumé. Cette contribution rapporte de nouvelles découvertes sur la pétrogenèse et l'emplacement géotectonique de rares dolérites subvolcaniques du Trias (?) présentes dans les Dinarides externes. Le but de cette étude est de contribuer au débat sur l'évolution géodynamique de la marge continentale de la (des) plate-forme(s) Adriatique-Dinaridique au début du Mésozoïque. La pétrographie des roches étudiées révèle l'ordre de cristallisation suivant : clinopyroxène → plagioclase → feldspath alcalin ± amphibole ± oxydes de Fe–Ti. La géochimie calco-alcaline de la dolérite suggère une génération de magma à partir d'une source de manteau péridotitique contenant du spinelle et du grenat (60sp :40grt). Deux mécanismes expliquant l'origine de la dolérite sont ici suggérés. Le premier implique une fusion partielle de bas degré du manteau lithosphérique altéré et de la lithosphère océanique modifiée par la subduction accompagnée de sédiments subduits. Le second propose une fusion du manteau lithosphérique subcontinental hétérogène contaminé ou métasomatisé par la subduction varisque au Paléozoïque supérieur. En conséquence, deux modèles géodynamiques sont suggérés : (i) une subduction vers le nord de type andin de la Paléotéthys au Trias moyen sous la marge continentale active laurasienne. Cette subduction était liée à la formation d'un arc volcanique péricontinental suivi d'un rifting d'arrière-arc, au sein de la plaque Adria, qui a conduit à la formation de systèmes de rifts localement avortés et à la subsidence de la plate-forme et (ii) une extension au Trias moyen de la nappe du Haut Karst dans la Grande Adria, non-affectée par une subduction, résultant d'un bref volcanisme syn-rift mettant en évidence la formation du système Dinarique de rift avorté suivie par la subsidence de la plate-forme et l'émergence de bassins sédimentaires locaux.

Keywords. Middle Triassic(?), Calc-alkaline subvolcanic rocks, Active continental margin, External Dinarides, Dolerite.

Mots-clés. Trias moyen (?), Roches subvolcaniques calco-alcalines, Marge continentale active, Dinarides externes, Dolérite.

Manuscript received 10 September 2022, revised and accepted 15 November 2022.

1. Introduction

The Dinarides stand for a 700 km long Alpine orogen consisted of high-karst mountains with a NW–SE extension, which connect the Southern Calcareous Alps (NW) and the Albanides (SE) [Dimitrijević, 1982, Pamić et al., 1998, Vlahović et al., 2005, 2012, Bortolotti et al., 2013, Figure 1a]. In the Triassic, the area of present-day Dinarides was located south of the northern margins of the subducting Paleotethyan lithosphere [Stampfli and Borel, 2002, 2003, Scotese, 2002]. During the Middle Triassic, the area of the Dinarides was affected by prominent tectonic processes which include wrench faulting, block tectonics and rifting [Schmid et al., 2008]. Repetitive uplifts and subsidence gave rise to the formation of deep marine environments marked by significant magmatic activity [e.g. Pamić and Balen, 2005]. The magmatism had its peak during the Ladinian [e.g. Pamić, 1984, Knežević et al., 1998, Trubelja et al., 2004, Pamić and Balen, 2005, Smirčić et al., 2018, 2020] and is related to the formation of Tethyan Mesozoic Adriatic-Dinaridic Carbonate Platform(s) [e.g. Castellarin et al., 1988, Philip et al., 1995, Vlahović et al., 2005, 2012, Robertson, 2007].

The Dinaridic mountain chain is made of thick and tectonized Carboniferous to Quaternary sedimentary successions [Pamić et al., 1998]. A plethora of Alpine tectonic events controlled the evolution of the Dinarides from the Late Permian to Oligocene; however, the most prominent event was the tectonic uplift and formation of an imbricated nappe system during the Late Eocene to Oligocene, which ultimately brought about a fold-and-thrust belt of the Dinarides [Pamić et al., 1998, Balling et al., 2021]. The Dinarides are consisted of the two parallel belts (Figure 1a): External Dinaridic platform and Internal Dinarides. The former includes the coastal mountain chains which stretch along the shores of the Adriatic, while the latter are found to the northeast extending parallelly to the former. External Dinarides are largely made of Jurassic to Cretaceous carbonate successions, which constitute the Adriatic Carbonate Platform [AdCP; Vlahović et al., 2005], while Internal Dinarides are consisted of deep-water sedimentary successions and ophiolite mélange obducted along

the margins of Adria Plate [Chiari et al., 2011, Dimitrijević and Dimitrijević, 1973, Pamić et al., 1998, Šegvić et al., 2014, 2019, 2020].

The occurrences of magmatic rocks in External Dinarides, i.e. the area of the Adriatic Carbonate Platform, are rarely reported, and if found, are small in surface cropping out at few localities solely (Senjska Draga, Donje Pazarište, vicinity of Sinj, Drniš and Knin, Fužinski Benkovac; Figures 1a and b). These basaltic, andesitic, dacitic, doleritic and gabbroic rocks may be found on some of the remote Adriatic islands such as Jabuka, Brusnik and Vis (Figure 1a); however, their origin has heretofore not been unequivocally defined especially with regards to geotectonic movements which caused the magmatism parental to those rocks [e.g. Barić et al., 1968, Barić, 1969, Golub and Vragović, 1975, Lugović and Majer, 1983, Pamić, 1984, Trubelja et al., 2004, Belak et al., 2005, Pamić and Balen, 2005, Garašić et al., 2005, 2006, De Min et al., 2009, Palinkaš et al., 2010, Smirčić, 2017]. Triassic effusive and associated volcanoclastic rocks are allochthonous and encountered in the fault zones along the rims of the Adriatic Carbonate Platform in contact with Anisian to Carnian sedimentary successions while intrusive rocks may crosscut Permian to Lower Triassic strata [Pamić, 1984, Pamić and Balen, 2005].

This study has a focus set on the biggest Triassic igneous subvolcanic body which crops out in the heart of External Dinarides in Croatia (Figure 1a–c). The body represents a unique manifestation of hypabyssal dolerite within the Adriatic Carbonate Platform. Its origin is related to the widespread magmatism having taken place along the rims of the AdCP which is documented by numerous occurrences of gabbroic rocks below Adriatic Sea [Mancinelli et al., 2022]. Assessing complex geodynamic processes and magmatic activity along AdCP continental rims the aim of this research is to advance our understanding on the extensional magmatism issued from subduction-modified mantle domains. This study brings new petrographic data, phase and rock geochemistry, as well Nd isotope systematics of investigated dolerite. From a mineralogical perspective this research offers an extensive characterization of the rare dolerite occurrence, while from the petrological point of view defines dolerite's geodynamic affinity, petrogenesis, as well as the intensity of plausible contamination and alteration processes. Petrogenetic inferences will be correlated with existing data collected from similar Triassic rocks cropping out throughout External Dinarides [Belak et al., 2005, Garašić et al., 2005, 2006, De Min et al., 2009, Palinkaš et al., 2010], Middle Triassic volcanic series from the Zagorje-Mid-Transdanubian Zone [Slovenec et al., 2020, Slovenec and Šegvić, 2021, Figure 1a] as well as Triassic volcanic rock from the Albanide-Hellenide belt [Pe-Piper and Panagos, 1989, Pe-Piper and Mavronichi, 1990, Capedri et al., 1997, Pe-Piper, 1998, Bortolotti et al., 2004, 2006, Monjoie et al., 2008, Chiari et al., 2012]. This will ultimately shed light on the influence of pre-Triassic subduction events on the composition of lithospheric mantle below the AdCP and add to the understanding of Mesozoic geodynamics of the central Mediterranean prior to the final disintegration of Pangea.

2. Geology of the study area

The location of the study area is in the south-western part of External Dinarides and belongs to the High Karst Unit [after Schmid et al., 2008; Figures 1a1 and a2]. The broader investigation area is geologically complex and according to Grimani et al. [1975] constitutes the Poštak-Plavno-Pađene tectonic unit, which is largely made of Triassic sedimentary series. Their lower bedding plane is made of Lower Triassic clastic and carbonate rocks represented by "Seissian beds" (shaley sandstone, oolithic/clayey limestone) and "Campilian beds" (platy limestone, marl, and dolomite). These rocks are overlain by Middle Triassic limestone and dolomite alternated by clastic and volcanoclastic rocks. The upper bedding plane of Triassic rocks is consisted of Upper Triassic dolomite transgressively overlain by Jurassic sediments (limestone and dolomite) of the Adriatic Carbonate Platform. Upper Cretaceous limestone is a next lithological member in this sequence found in a transgressive or tectonic contact with older rocks. Scarce occurrences of Paleogene carbonate-rich conglomerate and breccia are also documented transgressively overlying Upper Cretaceous rock series (Figure 1b).

Studied subvolcanic rocks crop out for about 300 m along the road at the southern entrance to the city of Knin (Northern Dalmatia, Croatia) (Figures 1a1, b1). These rocks are tectonically overlain

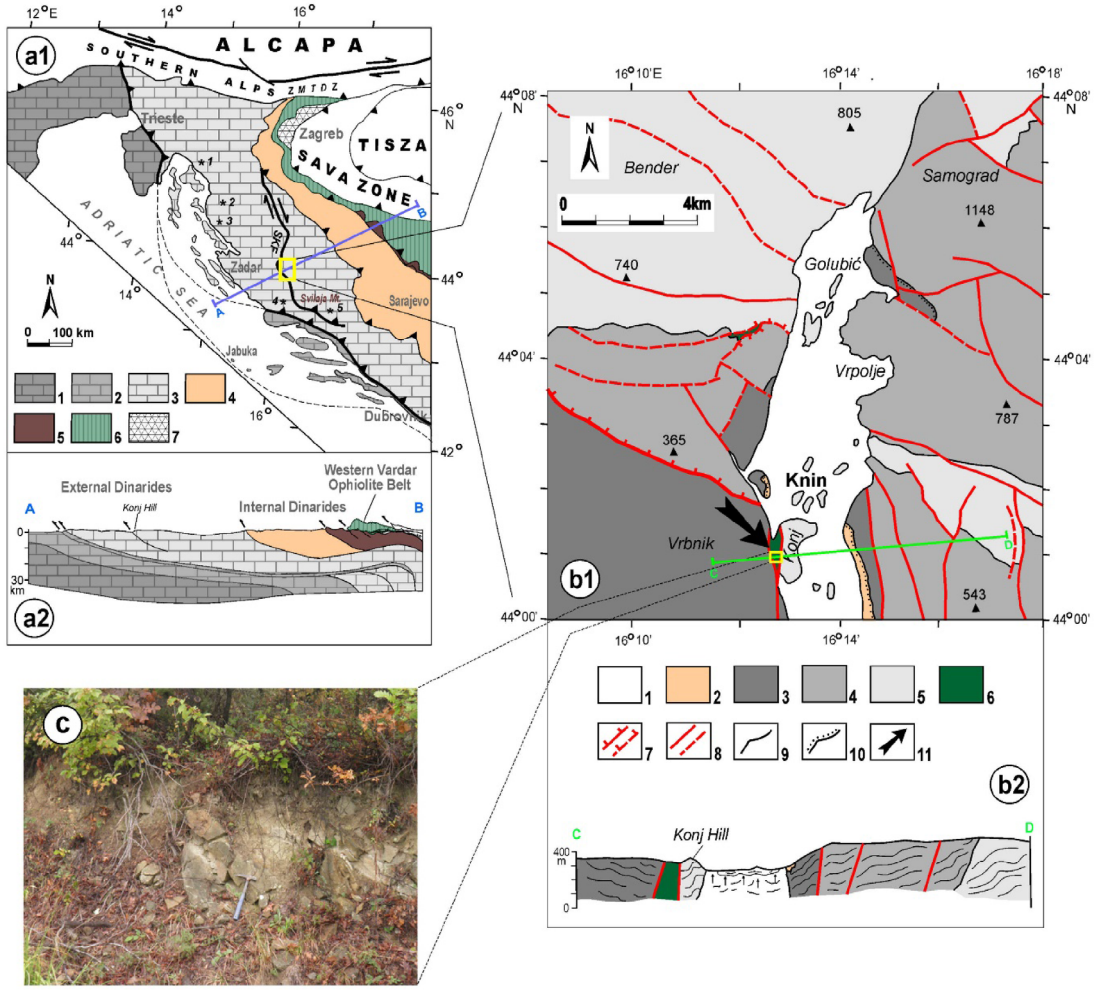

Figure 1. (a1) Geotectonic sketch map of the major tectonic units and (a2) schematic cross-section accros the Dinarides [simplified after Schmid et al., 2008, 2019]. Legend: External Dinarides: (1) Adriatic Plate, (2) Dalmatian Zone, (3) High Karst; Internal Dinarides: (4) Pre-Karst and Bosnian Flysch, (5) Drina-Ivanjica; (6) Meliata, Darnó-Sźarvaskö, Dinaric, Western Vardar, Mirdita; (7) Bükk, Jadar, Kopaonik. ZMTDZ—Zagorje-Mid-Transdanubian Zone, SKF—Split-Karlovac fault. The occurrences of magmatic rocks: (1) Fužinski Benkovac, (2) Donje Pazarište, (3) Senjska Draga, (4) vicinity of Drniš, (5) vicinity of Sinj. (b1) Simplified geological map of a wider research area and (b2) detailed cross-section [modified after Grimani et al., 1972, Kuljak, 2004]. Legend: (1) Quaternary sedimentary rocks; (2) Paleogene limestone conglomerates and breccias; (3) Early Cretaceous limestones; (4) Jurassic limestones and dolomites; (5) Triassic limestones, dolomites, clastic and volcanoclastic rocks; (6) subvolcanic rocks; (7) reverse or thrust faults; (8) normal faults; (9) normal geological line; (10) discordance line, tectonic-erosion discordance; (11) location of investigated area. (c) Field occurrence of the dolerite rocks in the study area.

by Late Cretaceous layered to blocky limestone and Early Triassic platy limestone ("Campilian beds"), while northwards the studied rocks are covered by Quaternary deposits (Figures 1b1, b2). The dolerite is found in the zone of the Split-Karlovac paleotransform fault [Chorowicz, 1975, 1977, Figure 1a1], along which Upper Permian evaporites break through [Bahun, 1985; Figures 1b1, b2]. The studied dolerite,

along with eruptive rocks from the region, was researched by Barić [1969], Grimani et al. [1975], and Kuljak [2004]; however, a detailed mineralogical, petrological and geochemical characterization is lacking. The age of magmatic activity parental to this magmatic occurrence has not been unequivocally determined as well. According to Grimani et al. [1975] it could be Pre-Triassic, likely corresponding to the Late Permian based off the age of the inclusions and identical heavy mineral fraction found in Upper Permian clastic rocks of the broader region [Ivanović et al., 1978, Šušnjara et al., 1992]. Middle Triassic (Ladinian) age cannot be excluded either considering a positive correlation with similar rocks at the neighboring mountain of Svilaja (Figure 1a) which are in a direct contact with Ladinian sediments [Ščavničar et al., 1984]. Bearing in mind such geological context and lack of datable igneous phases in dolerite this contribution favors its Middle Triassic age which is inferred for similar intrusive rocks at the Croatian Middle Adriatic islands [De Min et al., 2009]. Albeit cropping out at a relatively small surface, studied dolerite represents the most important primary occurrence of Middle Triassic(?) coarse grained mafic rocks in the central part of External Dinarides.

3. Materials and methods

3.1. *Materials*

Studied dolerite may be described as massive, brownish to greyish, heavily altered rock with an irregular to platy habit and visible ferromagnesian phases up to 4 mm in size (Figure 1c). Going toward the rims of the dolerite body the size of mineral grains abates because of rapid cooling of this hypabyssal, plausibly dyke-like type of rock. A set of 14 dolerite samples was selected for mineralogical, chemical and isotopic ($^{143}Nd/^{144}Nd$) analyses. All samples were firstly investigated with a petrographic microscope to define the rock's texture and modal mineralogy.

3.2. *Analytical techniques*

To determine mineral phase compositions of representative sample, we carried out the electron microprobe analyses and elemental X-ray study using a JEOL JXA 8200 Superprobe with a wavelength/energy dispersive combined microanalyzer installed at the University of Geneva, Switzerland. Operating parameters included an accelerating voltage of 20 kV, a 20 nA beam current, and a beam size of ~1 μm (for feldspars 10 μm). Counting times of 20 s on peak and 10 s on background on both sides of the peak were used for all elements. Limits of detection (LOD) were calculated as the minimum concentration required to produce count rates three times higher than the square root of the background (3 s; 99 wt% degree of confidence at the lowest detection limit). Raw data were corrected for matrix effects using the PAP algorithm implemented by JEOL [Pouchou and Pichoir, 1985]. Natural minerals, oxides (corundum, spinel, hematite, and rutile), and silicates (albite, orthoclase, anorthite, and wollastonite) were used for calibration. Mineral formulas were calculated using a software package MINPET written by Linda R. Richard (Gatineau QC, Canada).

Bulk-rock powders for chemical analyses of five samples were analyzed by ICP-OES for major elements, and ICP-MS for trace elements at Bureau Veritas Laboratories (Vancouver BC, Canada). International mafic rocks were used as standards. Major element and trace element concentrations were measured with accuracy and precision better than ±1% and ±5%, respectively. It is 3σ at 10 times detection limit.

Nd isotopic compositions of two bulk rock samples were measured at the Noble Gas Laboratory Pacific Centre for Isotopic and Geochemical Research, University of British Columbia, Vancouver, Canada, following the procedure described in Weis et al. [2006]. Collector cup bias was monitored by frequent measurement of the La Jolla Nd standard which yielded $^{143}Nd/^{144}Nd$ 0.511853 ± 11 (n = 6; fractionation corrected to $^{146}Nd/^{144}Nd$ = 0.7219). Python™ programing language (numpy package) was used to calculate the Monte Carlo propagation error through 10,000 iterations for $^{147}Sm/^{144}Nd$, $^{143}Nd/^{144}Nd(t)$ ratios.

X-ray diffraction (XRD) was carried out on a set of four representative samples. For that purpose, the material was firstly gently crushed and powdered in an agate mortar and was thereupon placed in the sample holder. The material was analyzed with a Bruker D8-Advanced diffractometer installed at Texas Tech University (Lubbock TX, USA) and run using a step scan in the Bragg–Brentano geometry with

CuKα radiation. The measurement settings were 45 kV and 40 mA with sample mounts scanned from 3 to 70 °2θ. Measurements were completed under air-dried conditions and at a counting time of 2.5 s per 0.02 °2θ. Lastly, the peaks of XRD patterns were interpreted and compared with the whole-rock geochemistry generated from ICP-MS to ensure geological fluidity. The Bruker EVA diffraction suite was used to analyze diffraction data.

4. Results

4.1. *Petrography and mineral chemistry*

Investigated subvolcanic rocks are medium to coarse grained and show nicely preserved igneous fabrics characterized by intergranular holocrystalline texture and homogenous structure (Figure 2) which classifies them as dolerite. The crystallization sequence includes: (a) sericitized and completely albitized subhedral to euhedral plagioclase ($An_{3.2–8.6}Ab_{89.8–95.7}Or_{0.4–4.1}$; Figures 2a–c, 3a; up to 1.2 mm in size) and less common alkali feldspar ($An_{0.2–1.0}Ab_{1.9–7.6}Or_{92.0–97.8}$; up to 1.0 mm in size), (b) subhedral diopside to augite ($Wo_{44.5–46.6}En_{37.1–45.3}Fs_{8.3–44.5}$; Figure 3b), (c) brown subhedral prismatic, weakly pleochroitic, igneous Ca-amphibole (tschermakite to pargasite; up to 4 mm in size; Figures 2b–d, 3c–d), (d) Fe–Ti oxide (magnetite?, titanite), and (e) opaque hematite/limonite. Apatite has been documented as a common accessory phase. While plagioclase has been thoroughly albitized, this process affected alkali feldspar only marginally (Figure 2e). Clinopyroxene is normally zoned and features a decrease in Mg#, Al^{VI}/Al^{IV}, Ca and Cr coupled with an increase in Ti towards the rims of the grains (Table 1). The Mg# is relatively high (75.6–87.2), while TiO_2 and Al_2O_3 abundances vary considerably (0.50–2.45 wt% and 0.76–6.56 wt%, respectively). Giret et al. [1980] has successfully utilized a $^{A}(Na+K)+^{B}(Ca+Na)$ vs. ^{T}Si ratio to discern between igneous and metamorphic amphibole; accordingly, analyzed amphibole is largely metamorphic with only a fraction of it considered as magmatic (Figure 3d). The latter is marked by lower Mg# (<57) and MgO concentrations (<11 wt%) on the one hand and higher Al_2O_3 (11.21–11.42 wt%) and FeO values (>16 wt%) on the other hand compared to the composition of the former (Table 1). Comparing Mg# values of primary pargasite and tschermakite with those of primary clinopyroxene a strong correspondence may be inferred (Table 1) which reflects their roughly coeval magmatic crystallization [Singh et al., 2016].

Studied dolerite is moderately altered with documented hydrothermal parageneses indicating pumpellyite–prehnite facies conditions [Figure 4a; Šegvić et al., 2022]. Four distinct alteration processes have been observed: (a) prehnitization and pumpellyitization of plagioclase giving rise to the formation of acicular aggregates of prehnite (Figures 2c, d; Table 2) and associated, but less common, microcrystalline acicular Al-pumpellyite (Figure 4a; Table 2), (b) chloritization of clinopyroxene and plagioclase leading to the formation of minute flakey trioctahedral Mg-chlorite of penninite composition (Figures 4b1, b2; Table 2), (c) alteration of clinopyroxene to form a secondary actinolite and tremolite (Figure 3c; Table 1) and (d) transformation of primary amphibole to Fe–Mg rich mica (Figure 2b–d). The pseudomorphosis of amphibole to biotite required an excess of K entering mineral structure while Ca, Na, and/or Mg vacated it at temperatures between 300 and 500 °C [Brimhall et al., 1985].

X-ray trace analyses showed dominance of amphibole, prehnite, albite and quartz. Pyrophyllite, chlorite and Fe–Mg mica (phlogopite and biotite) are less abundant. Traces of clinopyroxene were also documented. Chlorite, and to a lesser extent mica and phlogopite, show indications of post-peak hydrothermal activity or weathering in the form of smectite component mixed layering, which gave rise to the formation of chlorite–smectite.

4.2. *Geothermobarometric estimations*

Amphibole and clinopyroxene phase chemistry sheds light on their crystallization conditions; multiple inosilicate based geothermobarometers were thus employed to unveil at which pressure and temperature the studied dolerite formed. The geothermobarometer based on clinopyroxene composition [Putirka, 2008] yielded the maximal crystallization temperatures between 1205 and 1244 °C and pressures of 0.91–1.13 GPa, while the geobarometer of Nimis [1999] and Nimis and Ulmer [1998] returned similar equilibration pressures of 0.98 to 1.37 (±0.2) GPa. This corresponds to crystallization depths of Konj Hill dolerite of ~29 to 41 km.

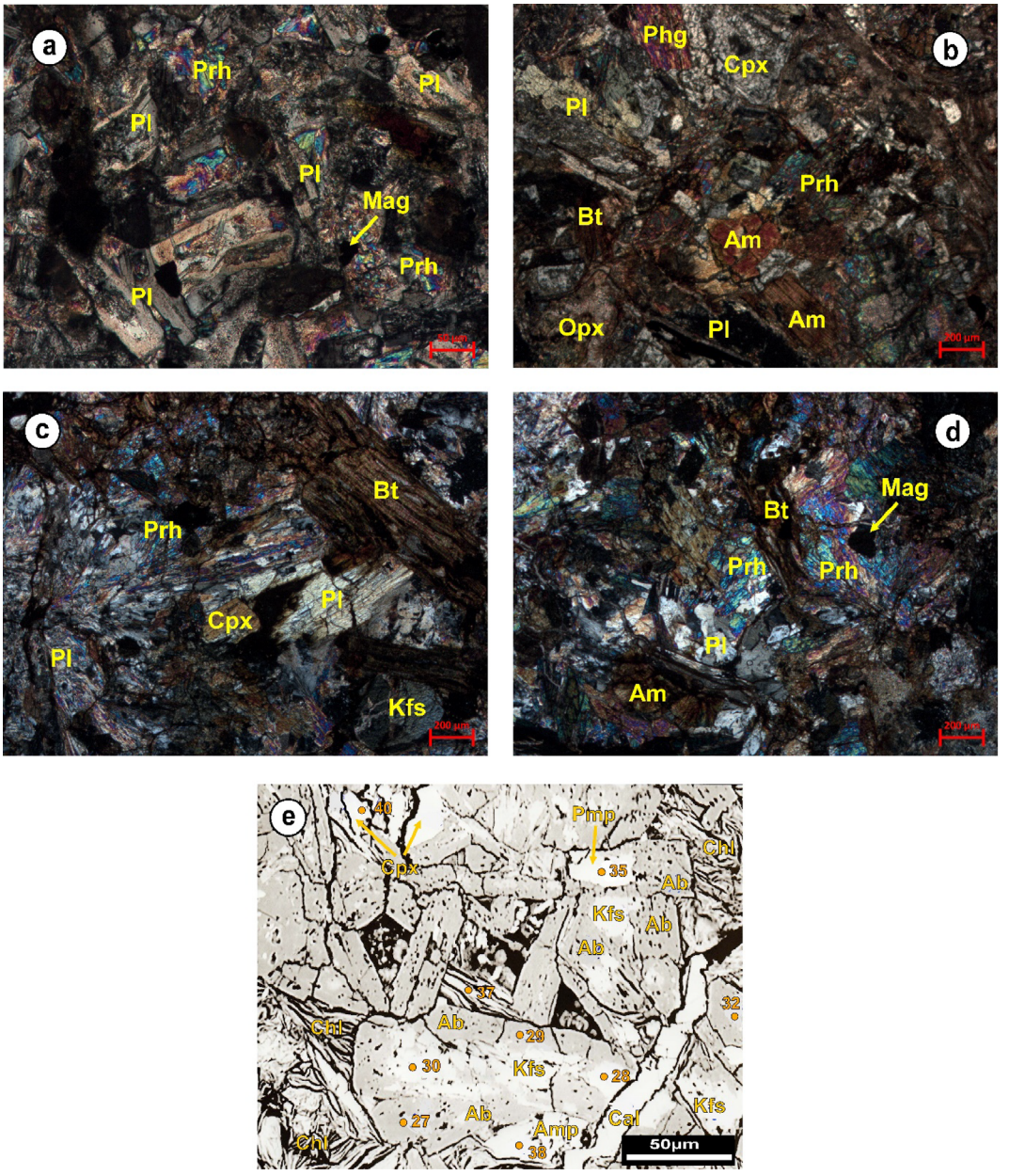

Figure 2. Microphotographs of thin sections of coarse-grained dolerite from the Konj Hill (a,b) sample KN-1, N+, (c,d) sample KN-4, N+ and back-scattered electron image of coarse-grained dolerite (e) sample KN-1. The numbers correspond to the microprobe spot presented in the Tables 1–2. Mineral abbrevations after Whitney and Evans [2010]: Ab—albite, Am—amphibole, Bt—biotite, Cal—calcite, Chl—chlorite, Cpx—clinopyroxene, Kfs—alkali feldspar, Mag—magnetite, Pl—plagioclase, Prh—prehnite, Pmp—pumpellyite.

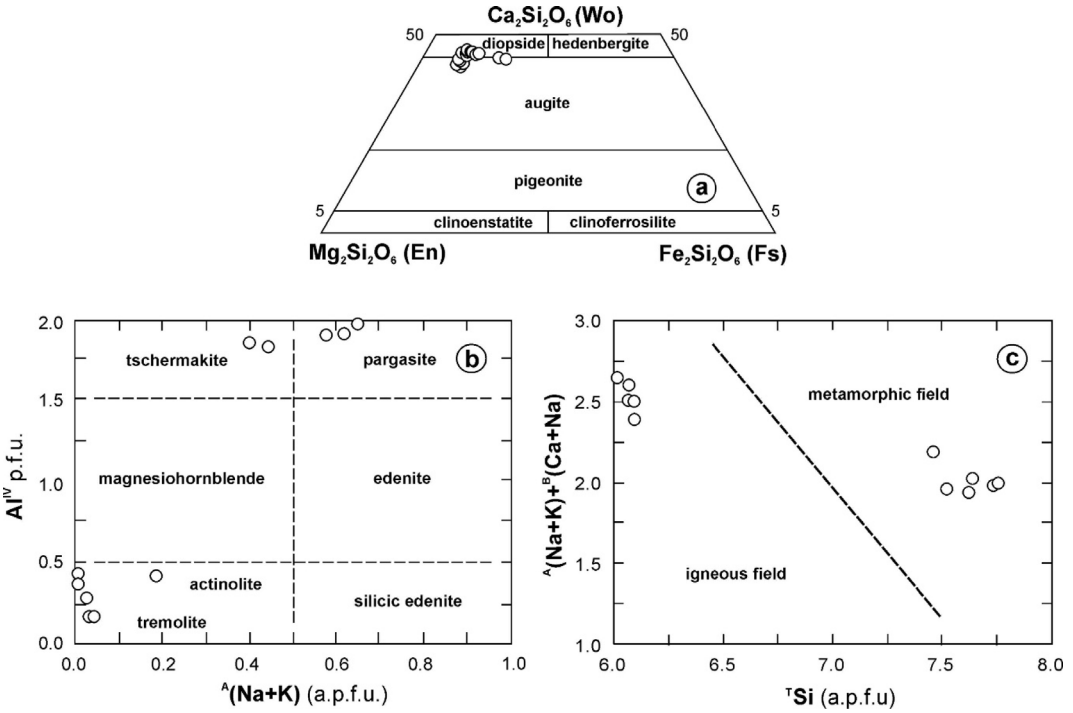

Figure 3. Classification diagrams for (a) pyroxene [En–Wo–Fs ($Mg_2Si_2O_6$–$Ca_2Si_2O_6$–$Fe_2Si_2O_6$) plot [Morimoto, 1988]], (b) calcium amphibole [Al^{IV}–^{A}(Na+K) plot [adapted after Leake et al., 1997, Hawthorne et al., 2012]] and (c) ^{A}(Na+K)+^{B}(Ca+Na)–^{T}Si discriminant diagram for amphibole [Giret et al., 1980].

Oxygen fugacity gives important insights in liquidus temperature and melt/crystal composition as well as magmatic processes in general [e.g. Kress and Carmichael, 1991, Botcharnikov et al., 2005, France et al., 2010]. The ratio of Al^{IV}+Na and Al^{VI}+2Ti+Cr of pyroxene may be used to draw illation on oxygen fugacity [Schweitzer et al., 1979]. The composition of analyzed pyroxene indicate high oxygen fugacity (Figure 5). This is likely an inheritance of the oxidized mantle source modified by fluids and/or melt derived from previously subducted Paleotethyan plate. The *P*–*T* conditions of the alteration processes were estimated based on the geochemistry of amphibole (formed by alteration of clinopyroxene) and chlorite. Based on the criteria of Schmidt [1992] amphibole crystallization pressures were set to the range from 0.20 to 0.25 GPa (±0.006 GPa). This corresponds to crystallization depths of ~6–8 km. Finally, the temperatures of chlorite formation were between 77.6 and 144.7 °C [Cathelineau, 1988, Jowett, 1991] and 81.9 to 99.7 °C [Kranidiotis and Maclean, 1987], which corresponds to very-low grade hydrothermal alteration processes.

4.3. *Whole-rock geochemistry*

Dolerite representative samples outline a comparable whole-rock chemical composition (Table 3). The concentrations of all measured elements vary in a very narrow span. The content of the most of macroelements is characteristic for mafic subvolcanic rocks [Cox et al., 1979, Chapter 2; Wilson, 1989, Chapters 5 and 7]; however, high MgO (9.28–10.31 wt%), CaO (up to 12.05 wt%) and LOI (8.70–11.57 wt%) coupled with low K_2O (<0.99 wt%) are typical characteristics of the investigated dolerite. Elevated LOI values reflect medium to high degrees of sea-floor alteration [Polat et al., 2002, Polat and Hofmann, 2003]. Dolerite samples were found to be SiO_2-undersaturated with the following CIPW normative abundances: anorthite (21–26%), diopside (16–32%), hypersthene (8–21%) and olivine (2–4%). The analyzed rocks are sub-alkaline calc-alkaline basalts (Figures 6a, b). They are characterized by high contents of Ni (202–239 ppm), Cr (592–768 ppm), Co (37–45 ppm) and Mg# (>70.3). Other compatible elements (e.g. Sc, Sr, V; Table 3) do not deviate

Table 1. Representative chemical compositions and calculated mineral formulae of clinopyroxene and amhibole from the mafic subvolcanic rocks (dolerites) from the Konj Hill

Mineral	Clinopyroxene								Amphibole						
Sample	KN-1	KN-1	KN-1	KN-1	KN-1	KN-1	KN-3	KN-3	KN-1	KN-1	KN-1	KN-1	KN-1	KN-1	KN-1
Anal. No.	2;c	3;r	5;r	15;c	16;r	40	49;r	53;c	38	41	42	43	44	45	54
Min. type	di	di	di	di	di	aug	di	aug	act/tr	prg	ts	act/tr	act/tr	act/tr	prg
SiO_2	51.28	50.41	50.58	50.85	49.94	46.53	51.20	52.67	53.20	40.56	40.56	54.97	54.91	54.50	39.22
TiO_2	0.68	1.01	0.99	1.04	1.13	2.45	0.72	0.50	0.15	3.89	2.57	0.36	0.26	0.25	3.87
Al_2O_3	3.36	4.24	3.88	4.32	4.67	6.56	3.31	1.76	2.42	11.42	11.21	1.15	1.06	1.05	11.40
Cr_2O_3	0.41	0.32	0.60	0.44	0.19	0.05	0.56	0.33	0.00	0.00	0.00	0.02	0.00	0.03	0.04
FeO	5.67	6.44	5.61	5.82	7.04	10.81	5.44	5.90	11.72	16.45	20.78	11.59	12.01	13.43	18.20
MnO	0.15	0.15	0.11	0.13	0.17	0.27	0.15	0.18	0.26	0.21	0.36	0.16	0.16	0.27	0.19
MgO	15.73	15.08	15.10	15.65	14.68	12.50	15.82	16.75	16.43	10.64	8.39	17.20	17.09	16.20	9.57
CaO	22.85	22.19	22.25	21.97	22.02	20.84	22.21	21.71	11.25	11.19	10.03	10.80	10.38	9.97	10.98
Na_2O	0.18	0.22	0.21	0.20	0.18	0.29	0.20	0.13	0.73	2.07	1.89	1.38	1.43	1.57	2.12
K_2O	0.01	0.00	0.00	0.00	0.00	0.02	0.01	0.01	0.05	1.17	1.13	0.15	0.20	0.18	1.17
H_2O	-	-	-	-	-	-	-	-	2.06	1.98	1.93	2.09	2.09	2.07	1.93
Total	100.32	100.04	99.32	100.51	99.93	100.33	99.61	99.94	98.27	99.56	98.85	99.87	99.59	99.51	98.68
Si	1.878	1.857	1.875	1.861	1.854	1.740	1.887	1.934	7.627	6.079	6.139	7.761	7.758	7.738	5.981
Ti	0.019	0.028	0.028	0.029	0.031	0.069	0.020	0.014	0.016	0.438	0.293	0.038	0.028	0.027	0.444
Al_{tot}	0.145	0.183	0.169	0.186	0.203	0.289	0.144	0.076	0.409	2.017	1.999	1.191	0.176	0.176	2.049
Al^{IV}	0.122	0.143	0.125	0.139	0.155	0.260	0.113	0.066	0.373	1.921	1.861	0.190	0.176	0.176	2.019
Al^{VI}	0.023	0.040	0.044	0.047	0.048	0.029	0.031	0.010	0.036	0.096	0.138	1.001	0.000	0.000	0.030
Cr	0.012	0.009	0.018	0.013	0.006	0.001	0.016	0.010	0.000	0.000	0.000	0.020	0.000	0.003	0.005
Fe^{3+}	0.063	0.053	0.023	0.036	0.052	0.113	0.041	0.029	0.637	0.530	1.120	0.537	0.682	0.793	0.654
Fe^{2+}	0.111	0.145	0.152	0.142	0.165	0.225	0.127	0.152	0.768	1.532	1.518	0.831	0.737	0.801	1.667
Mn	0.005	0.005	0.003	0.004	0.005	0.009	0.005	0.006	0.032	0.027	0.046	0.019	0.019	0.032	0.025
Mg	0.859	0.828	0.834	0.854	0.808	0.697	0.869	0.917	3.512	2.377	1.893	3.620	3.600	3.429	2.176
Ca	0.896	0.86	0.884	0.861	0.871	0.835	0.877	0.854	1.728	1.797	1.626	1.634	1.571	1.517	1.794
Na	0.013	0.016	0.015	0.014	0.013	0.021	0.014	0.009	0.203	0.601	0.555	0.378	0.392	0.432	0.627
K	0.000	0.000	0.000	0.000	0.000	0.001	0.000	0.000	0.009	0.224	0.218	0.027	0.036	0.033	0.228
Total	4.000	4.000	4.000	4.000	4.000	4.000	4.000	4.000	14.940	15.622	15.399	15.038	14.999	14.981	15.648
Mg#	80.56	85.09	84.58	85.74	83.04	75.59	87.24	85.78	82.06	60.81	55.49	81.33	83.01	81.06	56.62
Al^{VI}/Al^{IV}	0.19	0.28	0.35	0.34	0.31	0.11	0.27	0.15	-	-	-	-	-	-	-

Chemical compositions in wt%, mineral formulae in atoms per formula unit (apfu). act = actinolite; aug = augite; di = diopside; prg = pargasite; ts = tschermakite; tr = tremolite. Formulae calculated on the basis of 4 cations and 6 oxygens for clinopyroxene; 23 oxygens and 13 cats excluding Ca, Na and K for amphibole. Estimated H_2O corresponds 2 (OH) per formular unit for 1 amphibole. Mg# = 100 $*$ (Mg/(Mg+Fe^{2+})).

from the spans commonly reported in mafic volcanic/subvolcanic rocks [e.g. Wilson, 1989].

Zirconium on the one hand and high field strength elements (HFSE) and rare-earth elements (REE) (not shown) on the other hand outline well defined linear correlation which means that secondary remobilization of these elements was minimal. Conversely, large ion lithophile elements (LILE) show pronounced selective mobilization and will be therefore excluded from further petrogenetic considerations.

The N-MORB normalized element abundances feature uniform normalization patterns with significant enrichment in LILE (Cs, Rb, Ba and K) and Th compared to HFSE and mid- and heavy-rare-earth elements (MREE and HREE) at levels of 11 to 320 times relative to N-MORB (Figure 7a). Studied dolerite shows significantly pronounced negative anomalies of the Nb–Ta pair relative to La [$(Nb/La)_{N\text{-}MORB}$ = 0.39–0.43], as well as of Zr–Hf and Ti which is typical of subduction-related magmas [e.g. Pearce et al., 1984, Hofmann, 1997, Wang et al., 2016; Figure 7a]. A weak to moderate Pb anomaly relative to Ce [$(Pb/Ce)_{N\text{-}MORB}$ = 1.21–2.15] is another typical feature of studied rocks. The chondrite normalized REE patterns show moderate enrichment in light-rare-earth elements (LREE) over HREE [$(La/Lu)_{CN}$ = 8.09–8.53] at 31–60 times chondrite relative concentrations and nearly flat

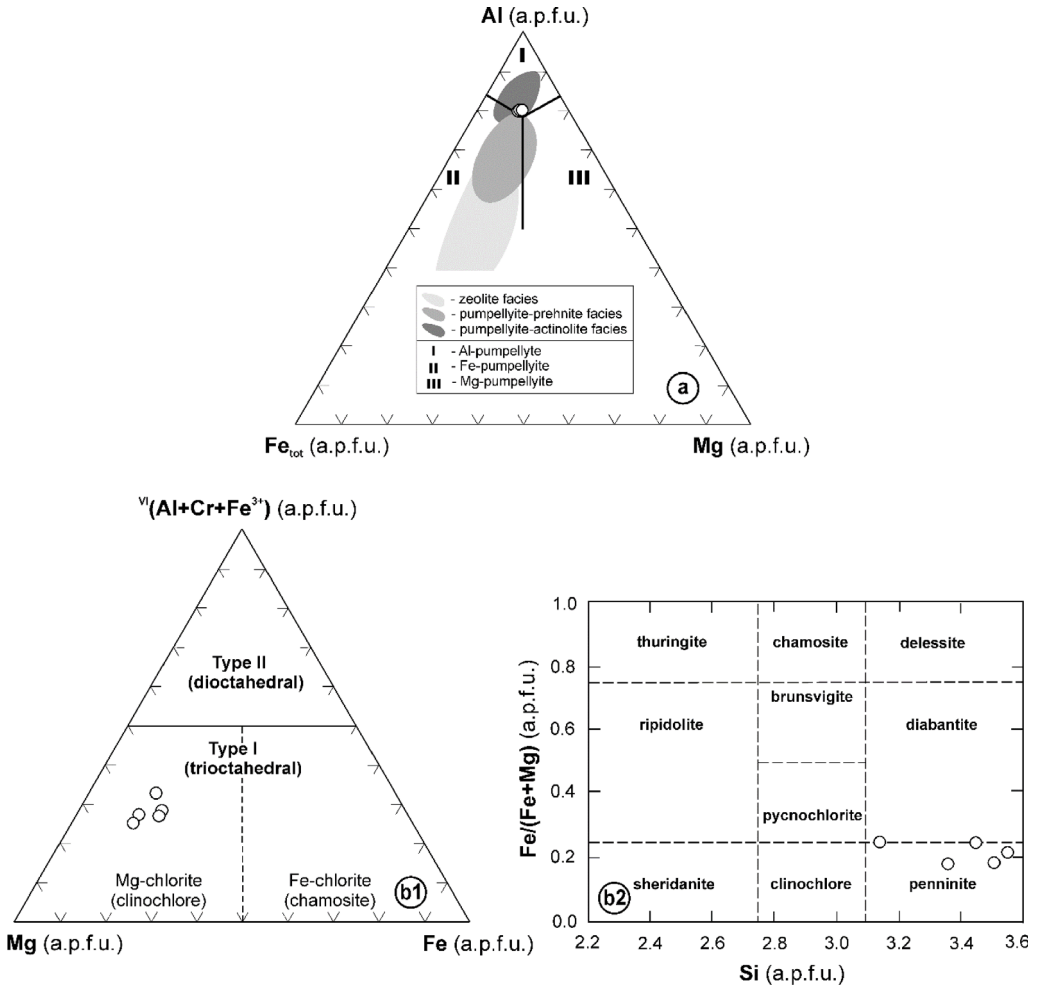

Figure 4. Classification diagrams for (a) pumpellyite [Fe$_{tot}$–Mg–Al plot [adapted after Passglia and Gottardi, 1973, Coombs et al., 1976]], the compositional fields of pumpellyite from the East Taiwan Ophiolite (zeolite facies), the Olympic Peninsula (prehnite–pumpellyite facies) and the Taveyannaz Formation (upper prehnite–pumpellyite and pumpellyite–actinolite facies) were taken from Mével [1981], Coombs et al. [1976] and Rahn et al. [1994]; chlorite (b1) Mg–Fe–^{VI}(Al+Cr+Fe^{3+}) diagram [Zane and Weiss, 1998]. (b2) Fe/(Fe+Mg)–Si diagram [after Hey, 1954 adapted to Sun et al., 2019] from subvolcanic rocks (dolerite) from the Konj Hill.

HREE profiles [(Tb/Lu)$_{CN}$ = 1.70–1.77] at 7–12 times relative to chondrite (Figure 7b). A low intensity of Eu anomaly (Eu/Eu* = 0.81–0.83) in dolerite samples marks an early fractionation of plagioclase.

The values of ^{143}Nd/^{144}Nd ratios of two representative dolerite samples fit a narrow span between 0.512352 and 0.512359 (Table 4). The initial ε_{Nd} are calculated for 242 Ma, which is the time of intensive volcanic activity in the larger area [Ščavničar et al., 1984]. The initial ε_{Nd} varies between −3.29 (±0.51) to −3.59 (±0.51). Values of ^{147}Sm/^{144}Nd and $\varepsilon_{Nd(t)}$ (Figure 8) are characteristic for the subduction of crustal derived material [SCM; Swinden et al., 1990].

5. Discussion

Middle Triassic(?) dolerite documented in the vicinity of the city of Knin in northern Dalmatia represents

Table 2. Representative chemical compositions and calculated mineral formulae of plagioclase, alkali-feldspar, prehnite, pumpellyite and chlorite from the mafic subvolcanic rocks (dolerites) from the Konj Hill

Mineral	Plagioclase			Alkali-feldspar			Prehnite			Pumpellyite		Chlorite		
Sample	KN-1	KN-1	KN-1	KN-1	KN-1	KN-1	KN-1	KN-1	KN-1	KN-1	KN-1	KN-1	KN-1	KN-1
Anal. No.	27	32	47	28	30	46	8	20	21	35	56	23	37	17
Min. type	ab	ab	ab	sa	sa	sa	-	-	-	Al-pmp	Al-pmp	pen	pen	pen
SiO_2	67.23	65.78	66.28	63.76	66.59	63.54	43.31	43.66	45.81	37.38	37.31	34.59	36.64	32.10
TiO_2	0.00	0.00	0.00	0.04	0.00	0.00	0.03	0.02	0.04	0.03	0.04	0.05	0.00	0.03
Al_2O_3	20.71	20.94	20.84	18.98	19.13	18.60	23.74	24.22	23.79	24.92	24.84	14.56	15.44	19.08
Cr_2O_3	0.00	0.00	0.00	0.00	0.00	0.00	0.00	0.00	0.02	0.00	0.00	0.06	0.03	0.00
FeO	0.12	0.41	0.45	0.08	0.12	0.28	0.37	0.21	0.37	5.16	5.25	12.53	10.22	12.98
MnO	0.00	0.00	0.00	0.03	0.00	0.00	0.03	0.11	0.00	0.19	0.17	0.08	0.03	0.19
MgO	0.00	0.00	0.00	0.02	0.02	0.00	0.00	0.00	0.00	2.35	2.31	21.07	20.37	21.56
CaO	0.82	1.47	1.86	0.20	0.04	0.07	26.57	26.57	24.16	22.43	22.51	1.23	1.48	0.48
Na_2O	11.73	10.91	10.77	0.43	0.21	0.83	0.00	0.01	1.03	0.03	0.02	0.05	0.19	0.03
K_2O	0.11	0.54	0.07	15.79	15.30	15.15	0.02	0.00	0.05	0.06	0.05	0.25	0.40	0.06
H_2O	-	-	-	-	-	-	4.72	4.76	4.83	6.47	6.46	11.87	12.13	12.14
Total	100.72	100.14	10.27	99.32	101.41	98.46	98.79	98.81	98.95	99.02	98.96	96.80	97.57	99.02
Si	2.931	2.900	2.909	2.966	3.007	2.977	3.026	3.022	3.130	3.034	3.032	3.447	3.551	3.138
Ti	0.000	0.000	0.000	0.000	0.000	0.000	0.002	0.001	0.002	0.002	0.002	0.004	0.000	0.002
Al_{tot}	1.063	1.087	1.077	1.040	1.017	1.026	1.955	1.976	1.916	2.384	2.379	1.734	1.800	2.221
Al^{IV}	-	-	-	-	-	-	-	-	-	-	-	0.553	0.449	0.861
Al^{VI}	-	-	-	-	-	-	-	-	-	-	-	1.181	1.351	1.360
Cr	0.000	0.000	0.000	0.000	0.000	0.000	0.000	0.000	0.001	0.000	0.000	0.004	0.003	0.000
Fe^{2+}	0.004	0.015	0.017	0.003	0.005	0.011	0.022	0.012	0.021	0.350	0.357	0.701	0.357	0.786
Fe^{3+}	0.000	0.000	0.000	0.000	0.000	0.000	0.000	0.000	0.000	0.000	0.000	0.342	0.471	0.274
Mn	0.000	0.000	0.000	0.001	0.000	0.000	0.002	0.006	0.000	0.013	0.012	0.007	0.003	0.016
Mg	0.000	0.000	0.000	0.001	0.001	0.000	0.000	0.000	0.000	0.284	0.280	3.130	2.943	3.142
Ca	0.038	0.069	0.087	0.010	0.02	0.004	1.989	1.971	1.769	1.950	1.960	0.131	0.153	0.051
Na	0.992	0.932	0.917	0.039	0.018	0.075	0.000	0.001	0.136	0.005	0.003	0.019	0.072	0.012
K	0.006	0.036	0.004	0.937	0.881	0.906	0.002	0.000	0.004	0.006	0.005	0.063	0.099	0.015
Total	5.034	5.039	5.011	4.998	4.931	4.999	6.996	6.996	6.980	8.028	8.030	9.582	9.452	9.657
An	3.67	6.65	8.63	1.01	0.22	0.41	-	-	-	-	-	-	-	-
Ab	95.75	89.88	90.97	3.95	1.99	7.61	-	-	-	-	-	-	-	-
Or	0.60	3.50	0.40	95.00	97.80	92.00	-	-	-	-	-	-	-	-
Mg#	-	-	-	-	-	-	-	-	-	-	-	81.7	89.2	79.9

Chemical compositions in wt%, mineral formulae in atoms per formula unit (apfu). Mineral formulae calculated on the basis of 8 oxygens and all Fe as Fe^{2+} for plagioclase and alkali-feldspar; 11 oxygens and all Fe as Fe^{2+} for prehnite; 12.25 oxygens and all Fe as Fe^{2+} for pumpellyite (H_2O is calculated and corresponds to 2 (OH) and 1.5 (OH) per formular unit in prehnite and pumpellyite, respectively); 14 oxygens and Fe as Fe^{2+} and Fe^{3+} for chlorite (H_2O is calculated and corresponds to 8 (OH) per formular unit). An = 100 ∗ Ca/(Ca+Na+K); Mg# = 100 ∗ (Mg/(Mg+Fe^{2+})). ab = albite; sa = sanidine; Al-pmp = aluminium pumpellyite, pen = penninite.

the biggest occurrence of mafic sub-volcanic rocks in the central part of External Dinarides. Its primary stratigraphic position with respect to the neighboring rocks (Figures 1b1, b2) cannot be unequivocally defined [Grimani et al., 1975]. A Middle Triassic affiliation to the volcano-sedimentary succession is, however, advised based on the correlation with coeval igneous rocks from the broader Dinaridic region [Ščavničar et al., 1984, De Min et al., 2009].

5.1. *Dolerite petrogenesis*

The origin of studied dolerite may be reconstructed based off the ratios of trace elements and Nd isotopic data. Generally, low values of Ba/Th and their steady increase coupled with the low $(La/Sm)_N$ (Figure 9) are in favor of a pervasive fluid metasomatism. The fluids likely originated from a previously subducted slab [Pearce, 1983, Plank, 2005]. Basaltic magmas affected by crustal contamination have La/Nb > 1.5,

Table 3. Chemical analyses of the mafic subvolcanic rocks (dolerites) from the Konj Hill

Sample	KN-1	KN-2	KN-3	KN-4	KN-5
SiO_2	42.85	42.36	43.18	44.51	44.62
TiO_2	1.08	1.11	0.99	0.98	0.86
Al_2O_3	11.57	11.43	11.72	12.17	12.24
Fe_2O_{3total}	8.27	8.01	8.16	8.04	8.32
MnO	0.16	0.15	0.15	0.16	0.16
MgO	10.24	10.31	9.86	9.34	9.28
CaO	12.16	12.18	12.10	12.10	12.05
Na_2O	1.24	1.31	1.42	1.55	1.59
K_2O	0.96	0.81	0.87	0.84	0.99
P_2O_5	0.23	0.24	0.21	0.20	0.19
LOI	10.70	11.57	10.86	8.70	9.13
Total	99.61	99.48	99.52	99.65	99.43
Mg#	72.27	72.41	71.51	70.39	70.26
Cs	2.4	2.5	2.4	2.3	2.2
Rb	32	34	29	28	27
Ba	248	251	232	227	221
Th	3.3	3.2	3.3	3.4	3.5
Ta	0.5	0.5	0.5	0.5	0.6
Nb	7.4	7.3	7.7	7.9	8.9
Sr	352	360	342	331	330
Zr	88	88	88	94	95
Hf	2.3	2.2	2.3	2.4	2.5
Y	18.3	18.1	19.2	21.3	21.8
Sc	26	25	26	26	27
V	205	207	203	201	200
Cr	760	768	721	596	592
Ni	237	239	212	209	202
Co	44	45	42	39	37
Pb	3.5	3.7	2.9	2.4	2.4
La	19.4	19.1	19.9	21.3	21.9
Ce	43.1	43.0	44.6	48.4	49.3
Pr	5.41	5.39	5.82	6.15	6.22
Nd	22.6	22.3	24.2	26.1	26.8
Sm	4.94	4.89	5.08	5.49	5.59
Eu	1.27	1.24	1.32	1.44	1.48
Gd	4.40	4.35	4.65	5.02	5.09
Tb	0.63	0.60	0.68	0.71	0.74
Dy	3.64	3.61	3.76	4.06	4.14
Ho	0.69	0.65	0.73	0.77	0.82
Er	1.97	1.92	2.21	2.27	2.33
Tm	0.26	0.25	0.27	0.29	0.30
Yb	1.58	1.56	1.68	1.71	1.74
Lu	0.23	0.22	0.24	0.26	0.27

Major elements in wt%, trace elements in ppm. LOI = loss on ignition at 1100 °C. Mg# = 100 ∗ molar ($MgO/(MgO+FeO_{total})$).

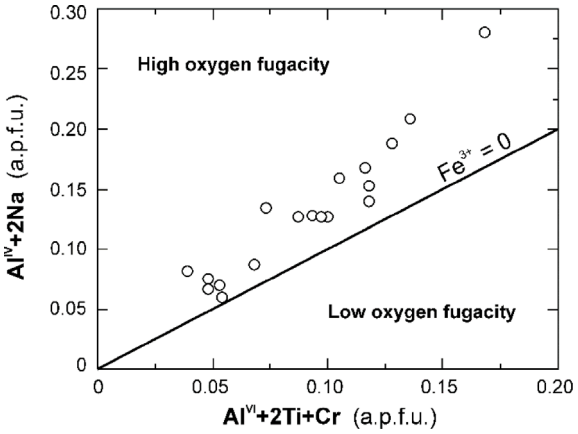

Figure 5. Oxygen fugacity condition of magma during clinopyroxene crystallization [Schweitzer et al., 1979].

La/Ta > 22, and K/P > 7 [Hart and Zindler, 1989]. Studied rocks however feature higher values of these ratios (La/Nb = 2.5–2.7; La/Ta = 36.5–42.6; K/P = 5.8–9.0) which suggests that their parental magmas experienced weak to moderate crustal contamination. A comparable degree of crustal contamination is inferred from elevated values of Th/Yb (1.82–1.88) and Th/Ta (5.8–6.8) as well as positive Pb spikes (up to 2.2; Figure 7a) [Taylor and McLennan, 1985]. Negative values of initial εNd (−3.29 to −3.59) accompanied by the very low values of $^{147}Sm/^{144}Nd$ ratio (≤0.126901; Figure 8) are in line with inferences on significant crustal interference. Advocated crustal contamination might have stemmed from a slow and prolonged magma uplift through the continental crust [e.g., Huppert and Stephen, 1985, Pomonis et al., 2004] and/or subducted/recycled sediments.

Balanced and high La/Yb_{PM} slopes (~15–17) as well as negative Zr–Hf anomalies (Figure 7a) may call for presence of residual garnet [Xie et al., 1993], which suggests that magmas that gave rise to the studied dolerite originated in the garnet-facies mantle. Using the Dy/Yb vs. Yb diagram (Thirwall et al., 1994; Figure 10) we therefore modelled the non-modal partial melting of a spinel peridotite, a garnet peridotite and a spinel–garnet peridotite mantle source. Accordingly, the studied rocks show a consistently narrow span along the evolution line for a spinel–garnet bearing peridotite mantle source (60sp:40grt) where partial melting likely ranged from

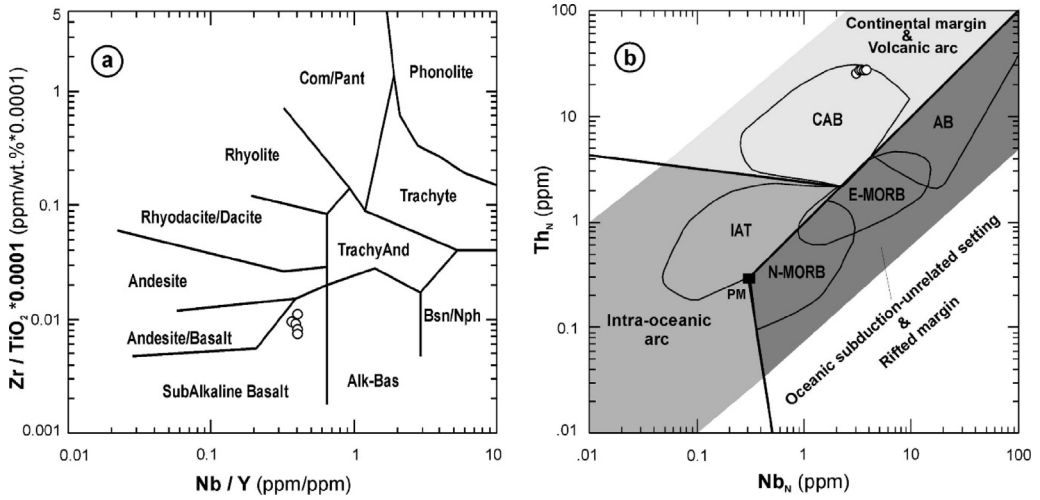

Figure 6. (a) Classification diagram $Zr/TiO_2 * 0.0001$–Nb/Y after Winchester and Floyd [1977], (b) Th_N–Nb_N discrimination diagram simplified after Saccani [2015] for the mafic subvolcanic rocks (dolerite) from the Konj Hill. Abbreviations: AB = alkali basalts; CAB = calc-alkaline basalts; E-MORB = enriched mid-ocean ridge basalts; IAT = island arc tholeiite; N-MORB = normal mid-ocean ridge basalts; PM = primitive mantle.

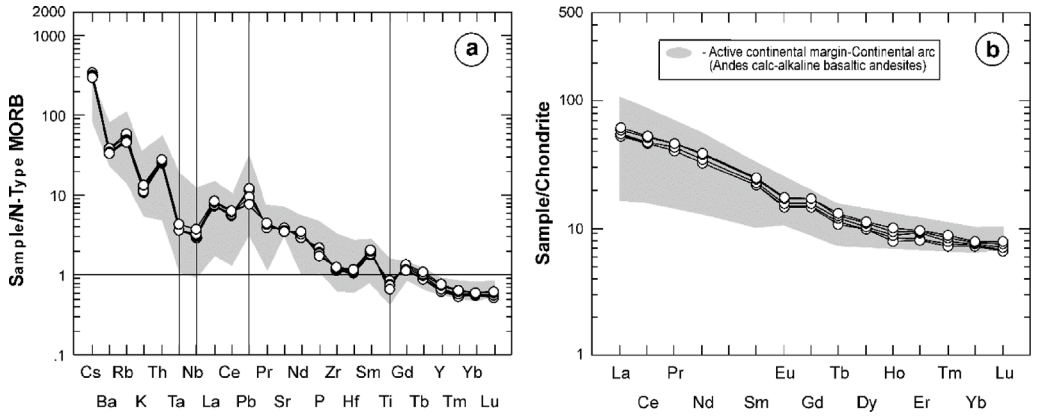

Figure 7. (a) N-MORB-normalized multielement and (b) REE patterns for the mafic subvolcanic rocks (dolerite) from the Konj Hill. Normalization values are from Sun and McDonough [1989]. Fields for active continental margin-continental arc calc-alkaline basaltic andesites in the Andes [Wilson, 1989, Chapter 7] are plotted for correlation constraints.

11 to 13%. This is corroborated by moderately elevated values of Sm/Yb_{PM} (3.1–3.3), which is indicative for melting in the spinel–garnet stability field. The above suggests the formation of melt in the garnet-facies, which was later mixed with the magmas generated at shallower mantle levels where residual spinel prevailed. This points out that studied rocks formed from a unique mantle source compared to similar Permian to Triassic igneous rocks cropping out elsewhere in External Dinarides and the Zagorje-Mid-Transdanubian Zone further to the north-west (Figures 1a and 10). To get more insights into the characteristics of studied rocks' mantle characteristics we utilized the Th/Yb vs. Ta/Yb discrimination diagram (Figures 11a, b). Enrichment in Th with regards to Ta and Yb indicates an origin from the

Table 4. Nd isotope data of the mafic subvolcanic rocks (dolerites) from the Konj Hill

Sample	Sm/Nd	$^{147}Sm/^{144}Nd$	$^{143}Nd/^{144}Nd$	$^{143}Nd/^{144}Nd_{(t)}$	$\varepsilon_{Nd(t)}$[a]	Time (t)[b]
KN-1	0.21858	0.132135 (7×10^{-3})	0.512352 (6×10^{-6})	0.512143 (3×10^{-5})	−3.59 (0.51)	242 ± 12.1 Ma
KN-3	0.20991	0.126901 (6×10^{-3})	0.512359 (6×10^{-6})	0.512158 (2×10^{-5})	−3.29 (0.51)	242 ± 12.1 Ma

Errors in brackets for Nd isotopic ratios are given at the 2σ-level. The method of calculating the errors is presented in the analytical techniques chapter. $^{147}Sm/^{144}Nd$ calculated from the ICP-MS concentrations of Sm and Nd following equation: $^{147}Sm/^{144}Nd = (Sm/Nd) * [0.53151 + 0.14252 * {}^{143}Nd/^{144}Nd]$. [a]Initial $\varepsilon_{Nd(t)}$ calculated assuming $I^{o}_{CHUR} = 0.512638$, $(^{147}Sm/^{144}Nd)^{o}_{CHUR} = 0.1966$, and $\lambda_{Sm} = 6.54\times10^{-12}$ a^{-1}. [b]Coresponding time for the initial ε_{Nd} and initial isotopic ratios for Nd.

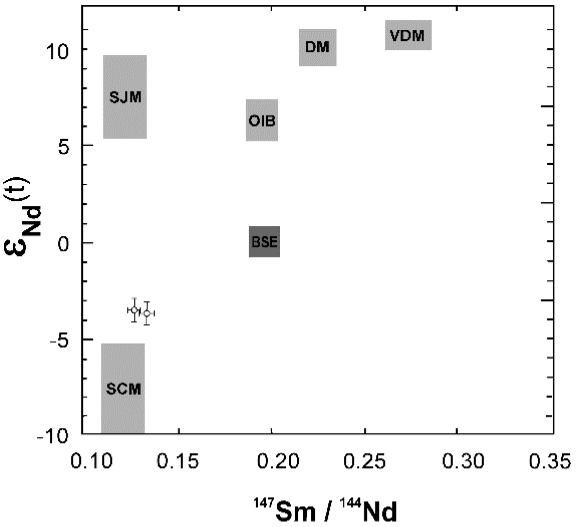

Figure 8. $^{147}Sm/^{144}Nd$—$\varepsilon_{Nd(240\ Ma)}$ diagram for the mafic subvolcanic rocks (dolerite) from the Konj Hill. Hypothetical mantle sources: DM—depleted mantle (not refractory), VDM—very depleted mantle (refractory), SJM—subducted juvenile material (subducted oceanic crust; slab with little pelagic sediment) and SCM—subducted continental material. The observed compositions and hypothetical end members sources calculated for the Middle Triassic following Swinden et al. [1990].

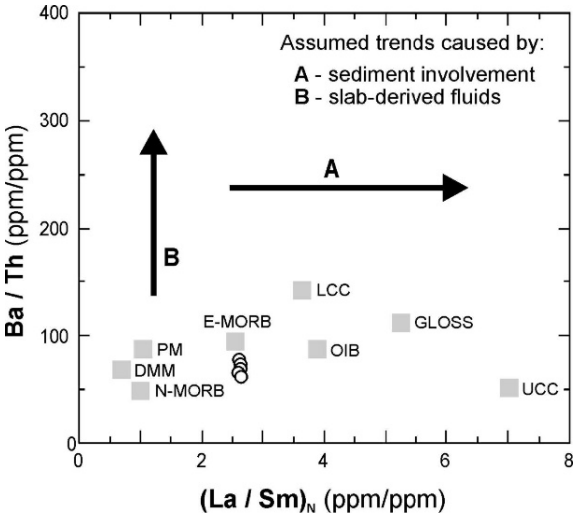

Figure 9. Ba/Th–(La/Sm)–N diagram [after Elliott, 2003] for the the mafic subvolcanic rocks (dolerite) from the Konj Hill. Abbreviations: [N-MORB = normal mid-ocean ridge basalts; E-MORB = enriched MORB; OIB = ocean island basalts; PM = primitive mantle [Sun and McDonough, 1989]]; [UCC = upper continental crust; LCC = lower continental crust [Taylor and McLennan, 1985]]; GLOSS = global subduction sediment [Plank and Langmiur, 1998]; DMM = depleted MORB mantle [Workman and Hart, 2005].

sources modified by subduction-related metasomatism [Pearce, 1982].

Considering high values of Mg# (>70), Ni (>200 ppm) and Cr (>500 ppm) measured in the investigated dolerite one may hypothesize its mantle origin; these values furthermore indicate the composition which corresponds to near-primary melt. In order to estimate melting conditions in the source the empirical model of Wood [2004] has been utilized. It relies on pressure, temperature, MgO and total alkalis in equilibrium with olivine, orthopyroxene and clinopyroxene. The estimations of melting pressures and temperatures thus vary from 0.86 and 1.21 (±0.33) GPa and 1265 and 1298 (±30) °C, respectively. This correlates well with the obtained *P*–*T* clinopyroxene conditions of 0.91 to 1.37 GPa and

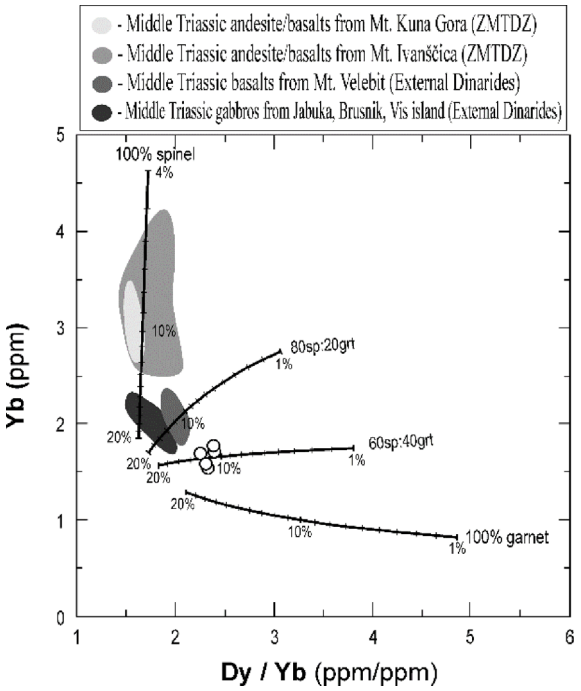

Figure 10. Yb–Dy/Yb diagram for the mafic subvolcanic rocks (dolerite) from the Konj Hill. Partial melting curves are shown for the non-modal batch melting of spinel and garnet lherzolite sources, starting from a Primitive Mantle [PM; McDonough and Frey, 1989] material. Mineral and melt modes for spinel and garnet-lherzolite source: $Ol_{0.58(0.10)}$ + $Opx_{0.27(0.27)}$ + $Cpx_{0.12(0.50)}$ + $Sp_{0.03(0.13)}$ [Kinzler, 1997] and $Ol_{0.60(0.05)}$ + $Opx_{0.21(0.20)}$ + $Cpx_{0.08(0.30)}$ + $Gt_{0.12(0.45)}$ [Walter, 1998], respectively. Italic numbers in parentheses indicate the percentages of each mineral entering the liquid. Partition coefficients are from McKenzie and O'Nions [1991].

1205 to 1244 °C, respectively. Mantle source(s) of such complex melts existed at depths between 26 and 41 km which corresponds to middle and upper segments of lithospheric mantle. A low Nb/La (0.37–0.41) corroborates their lithospheric origin [Smith et al., 1999].

In brief, one may hypothesize that analyzed dolerite was formed through complex processes of low-grade partial melting of the (a) subduction-modified oceanic lithosphere and/or subducted/recycled sediments beneath a metasomatically altered active mantle wedge and (b) lithospheric mantle which has been modified by the crustal component possibly during the melting of lower crustal material, (Figures 7a, 8 and 13a2). Alternatively, the investigated calc-alkaline rocks could have been generated by partial melting of subduction-modified heterogeneous hydrated lithospheric (subcontinental) mantle (Figure 13b2). This mantle portion had likely been contaminated and/or metasomatized during earlier Hercynian subduction events in the Late Paleozoic when local geotherms were raised due to passive upwelling of asthenospheric mantle along rifted margins (Figure 13b1).

5.2. *Tectonomagmatic significance*

To unveil tectonomagmatic provenance in which the studied rocks formed, the discrimination diagrams based on immobile trace elements and REE were utilized (Th_N–Nb_N, Hf/3–Th–Nb/16 and Th/Yb vs. Ta/Yb; Figures 6b, 11a, b). The studied dolerite was clearly formed in a subduction-related environment defined by a volcanic arc setting which evolved in an active, Andean-type, continental margin environment (Figure 12a). Further lines of evidence suggesting arc-related parental magmas are: (a) negative anomalies of Nb–Ta, Zr–Hf and Ti (Figure 7a) and retention of these elements in the slab [Pearce, 1982, 1983, Arculus and Powell, 1986, Hawkesworth et al., 1993, 1997, Wang et al., 2016], (b) normalization curves trends in chondrite-normalized REE diagrams (Figure 7b), and (c) clinopyroxene geochemistry (Figure 12b). Investigated dolerite rocks may therefore be classified as *orogenic* and are marked with typical calc-alkaline trends, which is a convergent geodynamic feature widely documented in the Dinarides, the Hellenides, and Southern Alps [Castellarin et al., 1988].

5.3. *Geodynamic significance*

Present paleogeographic reconstructions and geodynamic concepts of Triassic geology of the broader Mediterranean region suggested by Stampfli and Borel [2002, 2004] and Stampfli and Hochard [2009] on the one hand and van Hinsbergen et al. [2020] and van Hinsbergen and Schouten [2021] on the other hand show disagreements related to geotectonic

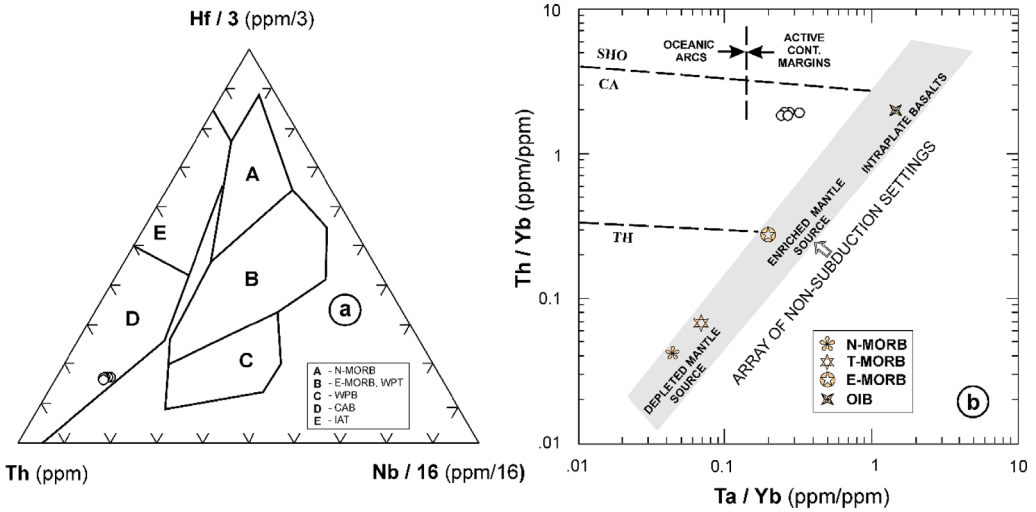

Figure 11. Discrimination diagrams for the mafic subvolcanic rocks (dolerite) from the Konj Hill. (a) Th—Nb/16–Hf/3 diagram [Wood, 1980]. A—normal mid-ocean ridge basalts (N-MORB); B—enriched MORB (E-MORB) and within-plate tholeiites (WPT); C—alkaline within-plate basalts (AWPB); D—calc-alkali basalts (CAB); E—island-arc tholeiites (IAT). (b) Ta/Yb—Th/Yb diagram [Pearce, 1983]. N-MORB, E-MORB and OIB are from Sun and McDonough [1989] and T-MORB are from Klein [2003].

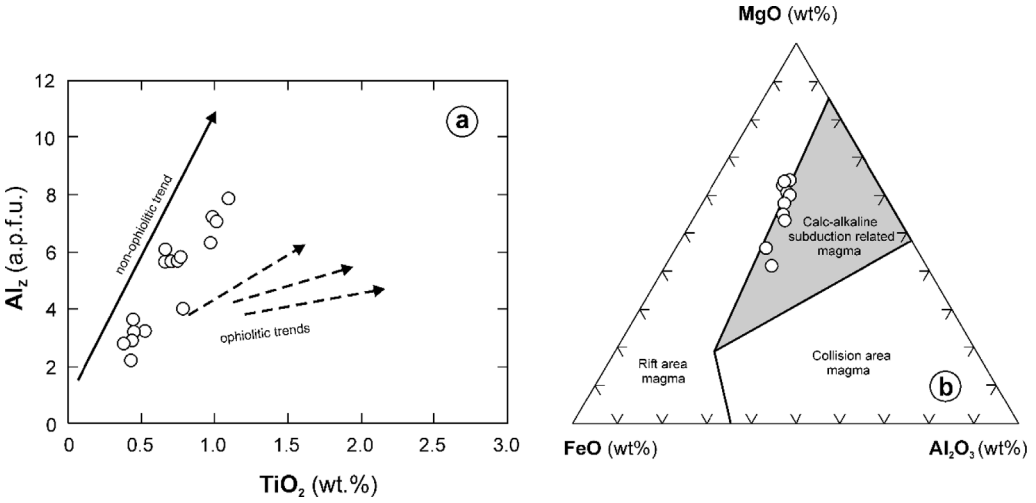

Figure 12. Discrimination diagrams (a) Al_Z (Al^{IV}*100/2)–TiO_2 [Loucks, 1990], (b) FeO–Al_2O_3–MgO [Le Bas, 1962] for pyroxene from the mafic subvolcanic rocks (dolerite) from the Konj Hill.

interpretations of geological events. Both concepts, however, include an active Middle to Late Triassic subduction of the Paleotethys to drive the Neotethyan ocean spreading (Figure 13). With reference to those two paleogeographic concepts (Figures 13a1, a3 and b1, b2) two geodynamic models are here proposed (Figures 13a2, a4 and b2, b4). They are based on different hypotheses of geotectonomagmatic interpretation:

(1) The geodynamic concept introduced by Stampfli and Borel [2002, 2004] and Stampfli and Hochard [2009] advocates Middle Permian to Middle Triassic north-directed subduction of the Paleotethys beneath the Laurasian (south European)

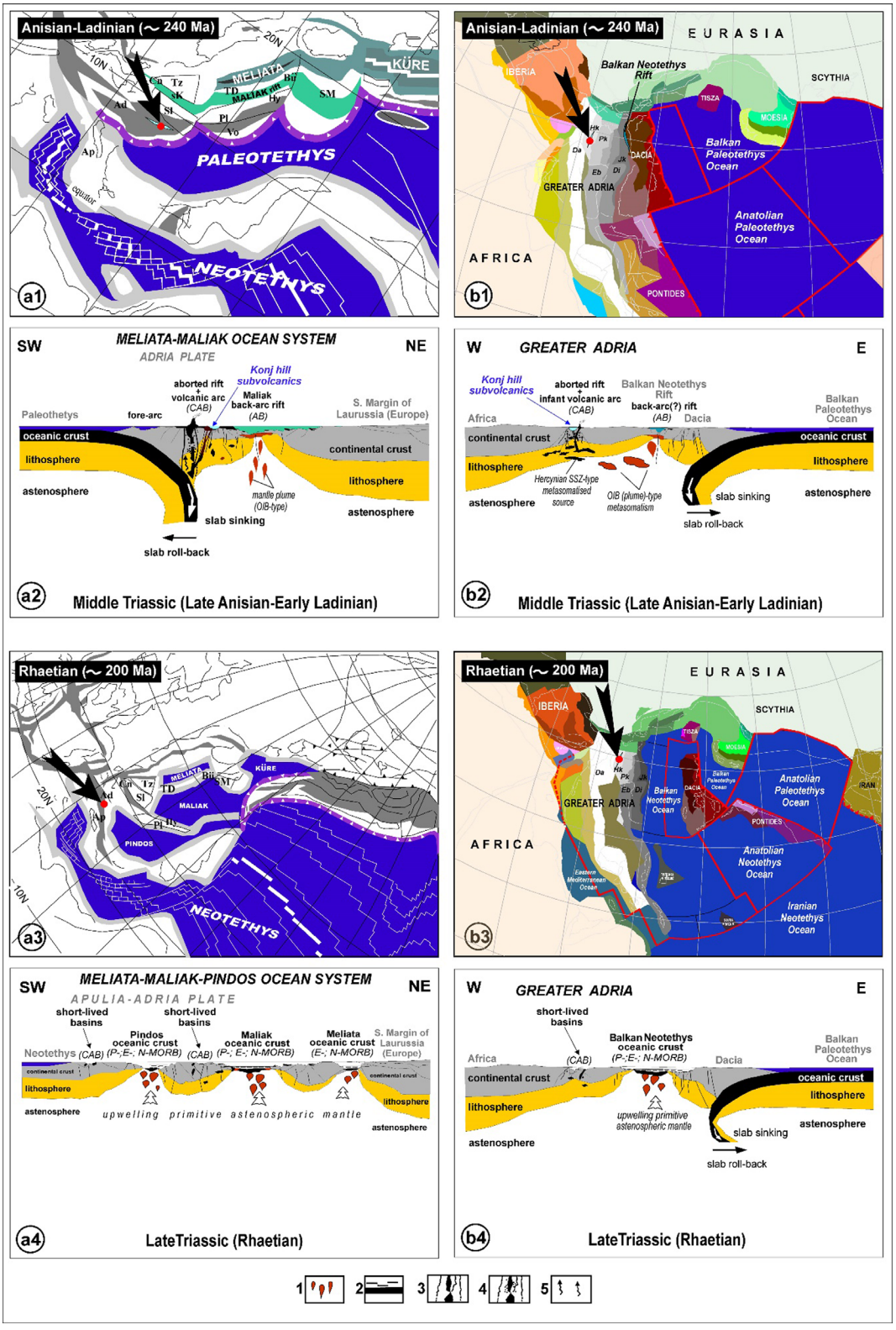

Figure 13. Caption continued on next page.

Figure 13. (**cont**.) Middle to LateTriassic palaeogeographic reconstruction of the Mediterranean region: (a1) Anisian–Ladinian (~240 Ma) and (a3) Rhaetian (~200 Ma) simplified after Stampfli and Borel [2004] [Ad = Adria Plate s. str., Ap = Apulia s. str., Bü = Bükk, Cn = Carnic-Julian, Hy = Hydra, Pl = Pelagonian, sK = south-Karawanken fore arc, Sl = Slavonia, SM = Serbo-Macedonian, TD = Trans-Danubian, Tz = Tisza, Vo = Vourinos (Pindos)] and (b1) Anisian–Ladinian (~240 Ma) and (b3) Rhaetian (~200 Ma) simplified and slightly modified after van Hinsbergen et al. [2020] [Da = Dalmatian Nappe, Di = Drina-Ivanjica Nappe, Eb = East Bosnian-Durmitor Nappe, Jk = Jadar-Kopaonik Nappe, Pk = Pre-Karst Nappe] with location of investigation area of Konj Hill (marked with black arrow and red dot symbol). Schematic geodynamic model (scale is approximate) for: (a2) interaction of active continental margin magmatic ativity (subduction-related ensialic volcanic arc magmatism) and roughly contemporaneous proto back-arc rifting and (a4) drifting to spreading of oceanic domain in Meliata-Maliak-Pindos ocean system [slightly modified after Slovenec et al., 2020] according to Stampfli and Borel [2004] palaeogeographic reconstruction shown in a1. (b2) Ensialic infant arc–back-arc rifting and (b4) spreading of oceanic domain in the central part of the Mediterranean region according to van Hinsbergen et al. [2020] palaeogeographic reconstruction shown in b1. *CAB* = calc-alkaline and shoshonitic basalts/volcaniclastites, *AB* = alkaline basalts, *OIB* = ocean island basalts, N-MORB = normal mid-ocean ridge basalts; E-MORB = enriched MORB; P-MORB = plume MORB; 1 = mantle diapires, 2 = oceanic crust topped by radiolarian cherts, 3 = partially melted previous subducted oceanic lithosphere, 4 = zone of partial melting and contamination by continental crust, 5 = fluids from previous subducted slab.

active margin followed by the final closure of this oceanic realm in the Late Triassic (Figure 13a1–a4). As a result, further to the north, several smaller rift belts and then back-arc basins [Meliata, Maliak, Pindos; e.g. Stampfli et al., 2013] came to being accompanied by the magmatism linked to an active subduction or rifting-related processes [Pe-Piper, 1998, Bortolotti et al., 2004, 2006, Neubauer et al., 2019, Lustrino et al., 2019, De Min et al., 2020]. These processes set path to Triassic magmatism and its intrusive, effusive and pyroclastic manifestations in the Dinarides, Albanides, Hellenides, Southern Alps and the Trans-Danubian region [Bébien et al., 1978, Castellarin et al., 1980, 1988, Pe-Piper and Panagos, 1989, Pe-Piper and Mavronichi, 1990, Capedri et al., 1997, Bortolotti et al., 2006, Monjoie et al., 2008, Obenholzner, 1991, Harangi et al., 1996, Trubelja et al., 2004, Smirčić et al., 2018, 2020, Lustrino et al., 2019, Slovenec et al., 2020, Slovenec and Šegvić, 2021]. One of such active Middle Triassic rifts within the Adria Plate stretched along the present day External Dinarides [Stampfli and Borel, 2003; Figure 13a1]. This extensional area therefore represents a back-arc rift basin of the Paleotethys which was subducted during the Triassic. This process was however halted already in the Ladinian because of regional geotectonic events which gave rise to the concept of the Dinaridic aborted rift [Smirčić, 2017]. Geochemical and isotopic data as well as mineralogy and petrogenesis of investigated dolerite are all in line with the geodynamic model connected to Middle Triassic northwards active(?) subduction of Paleotethyan lithosphere beneath the Laurussia (Figures 7, 11, 13a1–a2). Geochemical signatures of dolerite were likely inherited from the Paleotethyan subduction slab. Presented geochemistry is furthermore characteristic for Andean-type arc-related magmas of active continental margins [Wilson, 1989, Chapter 7]. This is in line with the inferences on the origin of Middle to Upper Triassic volcanic rocks in the Hellenides and Albanides [Pe-Piper and Panagos, 1989, Pe-Piper and Mavronichi, 1990, Capedri et al., 1997, Pe-Piper, 1998, Bortolotti et al., 2004, 2006, Monjoie et al., 2008, Chiari et al., 2012].

Dolerite parental magmas of the investigated rocks were likely generated at depths up to ~40 km and are related to upper to middle levels of lithospheric mantle. During the Late Anisian the west Paleotethys was characterized by passive upwelling of asthenospheric mantle, i.e. uplift of a mantle dome that, in turn, caused an adiabatic decompression along a system of subparallel faults [Slovenec et al., 2020]. In that sense the paleogeographic area of the Adria Plate and Dinarides experienced an extension coupled with subsidence which led to the formation of locally aborted rift systems which evolved

into a range of intracontinental basins behind the peri-continental volcanic arc [Vlahović et al., 2005, Smirčić, 2017, Smirčić et al., 2018]. The basins were prone to the accumulation of sedimentary material depending on the sea bathymetry. During Middle Triassic along one of those ephemeral and undeveloped aborted rift fault systems in External Dinarides investigated dolerite was crystallized (Figure 13a2). Finally, the regional geotectonic events during the Middle to Late Triassic in the area of External Dinarides dictated an abrupt closure of this passive syn-rift system which hence failed to evolve into an open ocean. Instead, a continuous terrigenous sedimentation ensued with a lack of magmatic activity after the Late Triassic time [Pamić and Balen, 2005, Vlahović et al., 2005, 2012].

It is important to note that during Middle Triassic time the arc-related magmatism of the southern active European continental margin was coeval with the proto back-arc rifting of the intracontinental lithosphere behind the pericontinental volcanic arc (Figure 13a2). The arc-related magmatism was however not genetically linked with the ophiolites generated in the Meliata-Maliak-Pindos back-arc basins. As a result of the upper Anisian uplift of mantle dome the carbonate platform gets disintegrated along the continental margin of the north-western segment of the Paleotethys. This was followed by the proto back-arc rifting of the intracontinental lithosphere behind the pericontinental volcanic arc [e.g. Slovenec et al., 2011; Figure 13a2]. The rifting produced uncontaminated primitive (OIB-type) alkali lavas free of crustal contamination (Figure 13a2). This calls for a significant rollback and retreat of the subducted sinking slab [Slovenec et al., 2010, 2011]. Further Middle-Late Triassic events in the western segment of Paleotethys included a terminal intracontinental rifting which prograded into an initial drifting and spreading of an ensialic back-arc basin [Slovenec et al., 2011; Figure 13a3–a4], which belonged to the larger Meliata-Maliak-Pindos Neotethyan oceanic system developed along the Laurasian (southern European) margin during Paleotethyan final subduction stages [Bortolotti et al., 2013, Stampfli et al., 2013, Stampfli and Borel, 2002, 2004]. The oldest spreading ridge oceanic crust related to the proto oceanization is represented by P-MORB-type and, thereafter, E-MORB-type volcanic rocks [e.g., Slovenec et al., 2011; Figure 13a4]. The newly formed oceanic realm in the western segment of Neotethys has continuously expanded during the Late Triassic and Early Jurassic leading to the formation of N-MORB-type oceanic crust. The occurrence of Middle-Late Triassic alkaline (OIB-type) and tholeiitic (P-, E-, N-MORB) volcanism in the Dinarides [e.g., Pamić, 1982, Vishnevskaya et al., 2009], in the Albanide-Hellenide belt [e.g. Pe-Piper and Panagos, 1989, Pe-Piper and Mavronichi, 1990, Capedri et al., 1997, Pe-Piper, 1998, Bortolotti et al., 2004, 2006, Monjoie et al., 2008, Chiari et al., 2012] and in the Bükk Mts. of Hungary [e.g., Harangi et al., 1996, Velledits, 2004, 2006] indicates a large-scale rifting of the continental lithosphere, followed by spreading and formation of the oceanic crust between the Apulia/Adria Plate and the continental margin of the southern Laurussia [e.g. Bortolotti et al., 2013, Saccani et al., 2015, and references therein].

(2) According to the geodynamic concept of van Hinsbergen et al. [2020] and van Hinsbergen and Schouten [2021] school of thoughts the basins and orogens of the Mediterranean region initiated the opening of the Eastern Mediterranean Ocean and the Balkan Neotethys Ocean during the early break-up of Pangea since the Triassic time. Beginning with the Jurassic these forms were obliterated through the subduction and terminal convergence between the African and Eurasian Plates. The opening of the Balkan Neotethys Ocean was a consequence of east-directed subduction of Balkan Paleotethys Ocean below the northeastern Adria/Dacia margin accompanied by the gradual northeastward roll-back of the Balkan Paleotethys slab (Figures 13b1 and b2). In such context the Mediterranean region represents the plate boundary zone between the African and Eurasian plates (Figure 13b1). With the opening of the oceanic basins in the area, the continental fragments separated from Eurasia and Gondwana were rifted and internally deformed into platforms and local basins [Dercourt et al., 1986, 2000]. The subduction of the oceanic and continental lithosphere was related to the stacking of upper crust at subduction plate boundaries, forming the regional nappe stacks of the Alps, the Carpathians, and the Dinaride-Hellenides, whereas their original lower crustal and mantle underpinnings had however subducted [Schmid et al., 2008, van Hinsbergen et al., 2005]. In that sense the Dinarides, as a part of the Greater Adria, placed within the North African margin, were

composed of several continental-derived nappes (Figure 13b1). One of those was the High Karst nappe characterized by shallow water Triassic sedimentation interrupted solely by a short episode of Middle Triassic deepening and rifting-related volcanism. This has led to subsidence and formation of the Dinaridic aborted rift [Smirčić, 2017]. Studied Middle Triassic (?) dolerite spatially associated with the High Karst unit, according to this geodynamic concept, characterize a syn-rift stage of the Dinaridic aborted rift (Figures 13b1 and b2).

The previous paragraph has shown that the origin of investigated dolerite, according to the model of van Hinsbergen et al. [2020] and van Hinsbergen and Schouten [2021] (Figure 13b1), may explain the petrogenetic model suggested by Saccani et al. [2015]. Contrary to the concept already discussed (proposed by Stampfli and Borel [2002, 2004] and Stampfli and Hochard [2009]; Figure 13a2) this alternative model (Figure 13b2) does not assume influence of an active subduction. This suggests that calc-alkaline rocks might have been generated by partial melting of the heterogeneous hydrated lithospheric (subcontinental) mantle metasomatized during older Variscan subductions. Late Paleozoic Hercynian subduction events which led to the formation of an Andean-type infant arc along the northwestern margin of Gondwana likely played an important role in hydrating the subcontinental lithospheric mantle [Pe-Piper, 1998]. An inference can therefore be made putting forth the formation of studied dolerite at the time of Middle Triassic extension and ephemeral syn-rift episode (Figure 13b2). The petrogenesis of dolerite is analogue to those of similar rocks found in the Albanide-Hellenide belt, especially with those from the southern Hellenides [Pe-Piper and Panagos, 1989, Pe-Piper and Mavronichi, 1990, Capedri et al., 1997, Pe-Piper, 1998, Monjoie et al., 2008, Chiari et al., 2012] and Southern Alps [e.g. Bonadiman et al., 1994, Lustrino et al., 2019]. Contemporaneous to Middle Triassic formation of calc-alkaline and shoshonitic rocks at the junction area of the Greater Adria and Dacia plates an initial rifting of intracontinental lithosphere took place (Figure 13b1–b2). The rifting was characterized by local passive upwelling and mixing of primitive asthenospheric mantle and metasomatized mantle producing OIB-type alkali lavas lacking a crustal contamination and that of the subducted Balkan Paleotethys slab. Later Middle to Late Triassic events in the area included an initial drifting and spreading (Figure 13b3–b4) which gave rise to the development of oceanic crust represented by P-MORB-type and then E-MORB-type and N-MORB-type volcanic rocks in the Dinaride-Albanide-Hellenide belt [e.g. Pamić, 1982, Capedri et al., 1997, Pe-Piper, 1998, Trubelja et al., 2004, Bortolotti et al., 2004, 2006, Monjoie et al., 2008, Vishnevskaya et al., 2009, Chiari et al., 2012, Koutsovitis et al., 2020]. The newly formed oceanic realm, known as the Balkan Neotethys Ocean [van Hinsbergen et al., 2020], progressively expanded during the Late Triassic and Early Jurassic time (Figure 13b3–b4).

Presented geodynamic models seem to be both acceptable; this study, however, gives preference to the second one that does not include a contemporaneous active subduction because, heretofore, there is no geological evidence in favor of its existence. Considering a high degree of resemblance of studied Dinaridic dolerite with its Triassic equivalents from the Albanide-Hellenide segment of Neotethys and extant geological data it is suggested that Triassic extension and ensuing incipient oceanization at the ocean-continent transition zones were not associated with a major mantle plume event or a contemporaneous active subduction [Pe-Piper, 1998].

6. Conclusions

- Subvolcanic calc-alkaline dolerite rocks that crop out in the vicinity of the city of Knin in the central part of External Dinarides belongs to the High Karst Unit.
- Petrography of the studied rocks revealed the crystallization order: clinopyroxene → plagioclase → alkali-feldspar ± Ca-amphibole ± Fe–Ti oxides.
- The estimations of melting pressure and temperature vary from 0.86 and 1.21 (±0.33) GPa and 1265 and 1298 (±30) °C, respectively. This is in line with P–T clinopyroxene conditions of 0.91 to 1.37 GPa and 1205 to 1244 °C, respectively. The mantle source(s) was suggested to have existed at depths between 26 and 41 km which corresponds to middle and upper segments of lithospheric mantle.

- Alteration hydrothermal processes indicating pumpellyite–prehnite facies conditions (P = 0.20–0.25 GPa (±0.006 GPa); T = 78–145 °C) at crystallization depths of ca. 6 to 8 km.
- As per geochemical and isotopic data of key incompatible trace elements the magmas which gave birth to analyzed dolerite likely separated from the garnet bearing mantle plume. Such melt(s) later mixed with the magmas generated at shallower mantle levels where residual spinel prevailed.
- Given the complexity of the petrogenetic processes and geotectonic environments of the origin of the investigated subvolcanic rocks, as well as the geodynamic concepts associated with them, two models are proposed: (1) analyzed dolerite was formed through processes of low-grade partial melting (11–13%) of the (a) subduction-modified oceanic lithosphere and/or subducted/recycled sediments beneath a metasomatically altered active mantle wedge and (b) lithospheric mantle modified by the crustal component during the melting of the lower crustal material (Figures 7a, 8 and 13a2).This model supports the geodynamic concept of Middle Triassic north-directed active subduction of the Paleotethys beneath the Laurasian active continental margin, which is accompanied by the formation of the pericontinental volcanic arc. In the arc marginal area, within the Adria Plate, an extension and back-arc rifting of the intracontinental lithosphere took place, which was followed by the emergence of locally aborted rift systems and subsidence of the platform (Figures 13a1, a2). (2) The investigated calc-alkaline rocks were generated by low-grade partial melting of the subduction-modified heterogeneous hydrated lithospheric (subcontinental) mantle (Figure 13b2), which was contaminated and/or metasomatized during earlier Variscan subduction events when local geotherms were raised due to the passive upwelling of asthenospheric mantle along the rifted margins (Figure 13b1). This model does not include an impact of a contemporaneous active subduction. Instead, it places the studied dolerite in the area of the Greater Adria where Middle Triassic extension of the High Karst nappe unit resulted with an ephemeral syn-rift volcanic phase and formation of the Dinaridic aborted rift system. Further platform subsidence ensued coupled with emergence of the local sedimentation basins (Figures 13b1, b2). Taken together, the results of this study are in favor of the second model.

Conflicts of interest

Authors have no conflict of interest to declare.

Acknowledgements

This work was supported by the Croatian Science Foundation under the project (IP-2019-04-3824). Kevin Byerly and Giovanni Zanoni are thanked for proofreading the manuscript. Critical comments and constructive reviews by two anonymous reviewers, as well as the editorial handling by Michel Faure, contributed significantly to the manuscript quality.

References

Arculus, R. J. and Powell, R. (1986). Source component mixing in the regions of arc magma generation. *J. Geophys. Res.*, 91, 5913–5926.

Bahun, S. (1985). Triassic deposits and Jelar Formation in the Una Valley between Srb and Brotnja (Croatia). *Geol. Vjesnik*, 38, 21–30.

Balling, P., Tomljenović, B., Schmid, S. M., and Ustaszewski, K. (2021). Contrasting along-strike deformation styles in the central external Dinarides assessed by balanced cross-sections: Implications for the tectonic evolution of its Paleogene flexural foreland basin system. *Glob. Planet. Change*, 205, article no. 103587.

Barić, L., Golub, L., and Vragović, M. (1968). Eruptive rocks of the northwestern part of Dalmatian Zagora. In Sokač, B., editor, *Zbornik Radova 3. Simposija Dinaridske Asocijacije = Proceedings of the 3th Simposium of Dinaridie Association*, pages 47–50. Zagreb (in Croatian, with an English abstract).

Barić, L. J. (1969). Eruptivne stijene (albitizirani dijabazi) iz okolice Sinja u Dalmaciji. *Geol. Vjesnik*, 22, 349–410. (in Croatian, with English abstract).

Bébien, J., Blanchet, R., Cadet, J. P., Charvet, J., Chorowitz, J., Lapierre, H., and Rampnoux, J. P. (1978). Le volcanisme triasique des Dinarides en Yougoslavie: sa place dans l'évolution géotectonique péri-méditerrenéenne. *Tectonophysics*, 47, 159–176.

Belak, M., Koch, G., Grgasović, T., Vlahović, I., Velić, I., Sokač, B., and Benček, Đ. (2005). Novi prinos stratigrafiji evaporitno-karbonatno-klastično-vulkanogenog kompleksa Komiškog zaljeva (otok Vis, Hrvatska). In Velić, I., Vlahović, I., and Biondić, R., editors, *Knjiga sažetaka 3. hrvatskog geološkog kongresa = Abstracts book of the 3th Croatian Geological Congress*, pages 13–14. Hrvatski geološki institut, Zagreb.

Bonadiman, C., Coltorti, M., and Siena, F. (1994). Petrogenesis and T-fO2 estimates of Mt. Monzoni complex (Central Dolomites, Southern Alps): a Triassic shoshonotic intrusion in a transcurrent geodynamic setting. *Eur. J. Mineral.*, 6, 943–966.

Bortolotti, V., Chiari, M., Kodra, A., Marcucci, M., Mustafa, F., Principi, G., and Saccani, E. (2004). New evidence for Triassic MORB magmatism in the northern Mirdita Zone ophiolites (Albania). *Ofioliti*, 29, 243–246.

Bortolotti, V., Chiari, M., Kodra, A., Martucci, M., Marroni, M., Mustafa, F., Prela, M., Pandolfi, L., Principi, G., and Saccani, E. (2006). Triassic MORB magmatism in the southern Mirdita zone (Albania). *Ofioliti*, 31, 1–9.

Bortolotti, V., Chiari, M., Marroni, M., Pandolfi, L., Principi, G., and Saccani, E. (2013). The geodynamic evolution of the ophiolites from Albania and Greece, Dinaric-Hellenic Belt: one, two, or more oceanic basins? *Int. J. Earth Sci.*, 102, 783–811.

Botcharnikov, R. E., Koepke, J., Holtz, F., McCammon, C., and Wilke, M. (2005). The effect of water activity on the oxidation and structural state of Fe in a ferro-basaltic melt. *Geochim. Cosmochim. Acta*, 69, 5071–5085.

Brimhall, G. H., Agee, C., and Stoffregen, R. (1985). The hydrothermal conversion of hornblende to biotite. *Can. Mineral.*, 23, 369–379.

Capedri, S., Toscani, L., Grandi, R., Venturelli, G., Papanikolaou, D., and Skarpelis, N. S. (1997). Triassic volcanic rocks of some type-localities from the Hellenides. *Chem. Erde*, 57, 257–276.

Castellarin, A., Lucchini, F., Rossi, P. L., Selli, L., and Simboli, G. (1988). The Middle Triassic magmatic-tectonic arc developed in the southern Alps. *Tectonophysics*, 146, 79–89.

Castellarin, A., Lucchini, F., Rossi, P. L., Simboli, G., Bosellini, A., and Sommavilla, E. (1980). Middle Triassic magmatism in southern Alps II: a geodynamic model. *Riv. Ital. Paleontol.*, 85, 3–4.

Cathelineau, M. (1988). Cation site occupancy in chlorites and illites as a function of temperature. *Clay Miner.*, 23, 471–485.

Chiari, M., Bortolotti, V., Marcucci, M., Photiades, A., Principi, G., and Saccani, E. (2012). Radiolarian biostratigraphy and geo-chemistry of the Koziakas massif ophiolites (Greece). *Bull. Soc. Géol. Fr.*, 183, 287–306.

Chiari, M., Djerić, N., Garfagnoli, F., Hrvatović, H., Krstić, M., Levi, N., Malasoma, A., Marroni, M., Menna, F., Nirta, G., Pandolfi, L., Principi, G., Saccani, E., Stojadinović, U., and Trivić, B. (2011). The geology of the Zlatibor-Maljen area (Western Serbia): A geotraverse across the ophiolites of the Dinaric-Hellenic collisional belt. *Ofioliti*, 36, 139–166.

Chorowicz, J. (1975). Le mécanisme de la structure transversale Split-Karlovac, dans les Dinarides yougoslaves. *C. R. Acad. Sci. Paris (D)*, 280, 2313–2316.

Chorowicz, J. (1977). *Étude géologique des Dinarides le Long de la Structure Transversale Split-Karlovac*. PhD thesis, Univ. Pierre et Marie Curie, Paris.

Coombs, D. S., Nakamura, Y., and Vuagnat, M. (1976). Pumpellyite-actinolite facies schist of the Taveyanne formation near Loeche, Valais, Switzerland. *J. Petrol.*, 17, 440–447.

Cox, K. G., Bell, J. D., and Pankhurst, R. J. (1979). *The Interpretation of Igneous Rocks*. George Allen and Unwin, London.

De Min, A., Jourdan, F., Marzoli, A., Renne, P. R., and Juračić, M. (2009). The tholeiitic Magmatism of Jabuka, Vis and Brusnik Islands: a Carnian magmatism in the Adria Plate. *Rend. Online Soc. Geol. Ital.*, 9, 85–87.

De Min, A., Velicogna, M., Ziberna, L., Chiaradia, M., Alberti, A., and Marzoli, A. (2020). Triassic magmatism in the European Southern Alps as an early phase of Pangea break-up. *Geol. Mag.*, 157, 1800–1822.

Dercourt, J., Gaetani, M., and Vrielynck, B. (2000). *Atlas Peri-Tethys Palaeogeographical Maps*. Commission de la Carte Géologique du

Monde/Commission for the Geological Map of the World, Paris, France.

Dercourt, J., Zonenshain, L. P., Ricou, L. E., Kazmin, V. G., Le Pichon, X., Knipper, A. L., Grandjacquet, C., Sbortshikov, I. M., Geyssant, J., and Lepvrier, C. (1986). Geological evolution of the Tethys belt from the Atlantic to the Pamirs since the Lias. *Tectonophysics*, 123, 241–315.

Dimitrijević, M. D. (1982). Dinarides: an outline of tectonics. *Earth. Evol. Sci.*, 2, 4–23.

Dimitrijević, M. D. and Dimitrijević, M. N. (1973). Olistostrome Mélange in the Yugoslavian Dinarides and Late Mesozoic Plate Tectonics. *J. Geol.*, 81, 328–340.

Elliott, T. (2003). Tracers of the slab. In Eiler, J., editor, *Inside the Subduction Factory, Geophysical Monograph*, volume 138, pages 23–45. AGU, Washington DC.

France, L., Ildefonse, B., Koepke, J., and Bech, F. (2010). A new method to estimate the oxidation state of basaltic series from microprobe analysis. *J. Volcanol. Geochem.*, 69, 61–120.

Garašić, V., Krkač, M., Lugović, B., Tadej, N., Vrkljan, M., Đomlija, P., Garapić-Šiftar, G., and Majer, V. (2006). Petrological characteristics of Ladinian magmatic rocks from the External Dinarides (Vratnik, Croatia). In Altherr, R., editor, *Berichte der Deutschen Mineralogischen Gesellschaft*, volume 18, pages 44–44. Beih. Z. Eur. J. Mineral, Stuttgart.

Garašić, V., Vrkljan, M., Tadej, N., Majer, V., Đomlija, P., and Garapić Šiftar, G. (2005). Volcanic Rocks of the Island Vis (Adriatic Sea, Croatia). Knjiga sažetaka 3. In Velić, I., Vlahović, I., and Biondić, R., editors, *Hrvatski geološki kongres = Abstract Book 3rd Croatian Geological Congress*, pages 37–38. Hrvatski geološki institut, Zagreb.

Giret, A., Bonin, B., and Leger, J. M. (1980). Amphibole compositional trends in over saturated and undersaturated alkaline plutonic ring complexes. *Can. Mineral.*, 18, 481–485.

Golub, L. and Vragović, M. (1975). Eruptive rocks of Dalmatian islands (Vis, Jabuka i Brusnik). Prirodoslovna istraživanja 41, Zagreb. *Acta Geol.*, 8, 19–63. (in Croatian, with English abstract).

Grimani, I., Šikić, K., and Šimunić, A. (1972). Basic geological map SFRJ 1:100 000, sheet Knin (L 33-141). Institut za geološka istraživanja Zagreb, Savezni geološki zavod Beograd.

Grimani, I., Šikić, K., and Šimunić, A. (1975). Basic geological map SFRJ 1:100 000. Explanatory notes for sheet Knin (L 33-141). Institut za geološka istraživanja Zagreb, Savezni geološki zavod Beograd, 61p. (in Croatian).

Harangi, S., Szabó, C., Józsa, S., Szoldán, Z., Árva-Sós, E., Balla, M., and Kubovics, I. (1996). Mesozoic igneous suites in Hungary: Implications for genesis and tectonic setting in the northwestern part of Tethys. *Int. Geol. Rev.*, 38, 336–360.

Hart, S. and Zindler, A. (1989). Constraints on the nature and development of chemical heterogeneities in the mantle. In Peltier, W. R., editor, *Mantle Convection*, pages 216–387. Gordon and Breach Science Publishers, New York.

Hawkesworth, C. J., Gallagher, K., Hergt, J. M., and McDermott, F. (1993). Trace element fractionation processes in the generation of island arc basalts. In Cox, K. G., McKenzie, D. P., and White, R. S., editors, *Melting and Melt Movement in the Earth. Philosophical Transactions of Royal Society*, volume A342, pages 179–191. Oxford University Press, London.

Hawkesworth, C. J., Turner, S. P., McDermott, F., Peate, D. W., and Van Calsteren, P. (1997). U-Th isotopes in arc magmas: implications for element transfer from the subducted crust. *Science*, 276, 551–555.

Hawthorne, F. C., Oberti, R., Harlow, G. E., Maresch, W. V., Martin, R. F., Schumacher, J. C., and Welch, M. D. (2012). Nomenclature of the amphibole supergroup. *Am. Mineral.*, 9, 2031–2048.

Hey, M. H. (1954). A new review of the chlorites. *Min. Mag.*, 30, 277–292.

Hofmann, A. W. (1997). Mantle geochemistry: the message fromoceanic volcanism. *Nature*, 385, 219–229.

Huppert, H. E. and Stephen, R. J. (1985). Cooling and contamination of mafic and ultramafic magmas during ascent through continental crust. *Earth Sci. Planet. Lett.*, 74, 371–386.

Ivanović, A., Sikirica, V., Marković, S., and Sakač, K. (1978). Basic geological map SFRJ 1:100 000. Explanatory notes for sheet Drniš (K 33-9). Institut za geološka istraživanja Zagreb, Savezni geološki zavod Beograd, 60 pages (in Croatian).

Jowett, E. C. (1991). Fitting Iron and Magnesium into the Hydrothermal Chlorite Geothermometer. In *Abstracts of the GAC/MAC/SEG Joint Annual Meet-*

ing (Toronto, May 27–29, 1991), volume 16, page A62.

Kinzler, R. J. (1997). Melting ofmantle peridotite at pressure approaching the spinel to garnet transition: application to mid-ocean ridge basalt petrogenesis. *J. Geophys. Res.*, 102, 853–874.

Klein, E. M. (2003). Geochemistry of the igneous oceanic crust. In Holland, H. D. and Turekian, K. K., editors, *Treatise on Geochemistry*, volume 3, pages 433–463. Elsevier, Amsterdam.

Knežević, V., Jovanović, V., Memović, E., and Resimović, K. (1998). Triassic magmatic rocks of Yugoslav Dinarides – in Serbia. Eruptive rocks of Dalmatian islands. In *XIII kongres geologa Jugoslavije, Herceg Novi, Zbornik radova*, volume 3, pages 61–66.

Koutsovitis, P., Magganas, A., Ntaflos, T., Koukouzas, N., Rassios, A. E., and Soukis, K. (2020). Petrogenetic constraints on the origin and formation of the Hellenic Triassic rift-related lavas. *Lithos*, 368–369, article no. 105604.

Kranidiotis, P. and Maclean, W. H. (1987). Systematicos f Chlorite Alteration at the Phelps Dodge Massive Sulfide Deposit, Matagami. *Quebec. Econ. Geol.*, 82, 1898–1911.

Kress, V. C. and Carmichael, I. S. E. (1991). The compressibility of silicate liquids containing Fe_2O_3 and the effect of composition, temperature, oxygen fugacity and pressure on their redox states. *Contrib. Mineral. Petrol.*, 108, 82–92.

Kuljak, G. (2004). *Geology of evaporites and accompanying rocks in Kosovo Polje near Knin*. MSc thesis, Zagreb University. 86 p. (in Croatian, with English abstract).

Le Bas, M. J. (1962). The role of aluminium in igneous clinopyroxene with relation to their parentage. *Am. J. Sci.*, 260, 267–288.

Leake, B. E., Woolley, A. R., Arps, C. E. S., Birch, W. D., Gilbert, M. C., Grice, J. D., Hawthorne, F. C., Kato, A., Kisch, H. J., Krivovichev, V. G., Linthout, K., Laird, J., Mandarino, J. A., Maresch, W. V., Nicke, L. E. H., Rock, N. M. S., Schumacher, J. C., Smith, D. C., Stephenson, N. C. N., Ungaretti, L., Whittaker, E. J. W., and Youzhi, G. (1997). Nomenclature of amphiboles: Report of the Subcommitte on Amphiboles of the International Mineralogical Association, Commission on New Minerals and minerals names. *Am. Mineral.*, 82, 1019–1037.

Loucks, R. R. (1990). Discrimination of ophiolitic from nonophiolitic ultramafic-mafic allochthons in orogenic belts by the Al/Ti ratio in clinopyroxene. *Geology*, 18, 346–349.

Lugović, B. and Majer, V. (1983). Eruptivi Senjske drage (Vratnik) kod Senja (SR Hrvatska, Jugoslavija). *Geol. Vjesnik*, 36, 157–181.

Lustrino, M., Abbas, H., Agostini, S., Gaggiati, M., Carminati, E., and Gianolla, P. (2019). Origin of Triassic magmatism of the Southern Alps (Italy): constraints from geochemistry and Sr-Nd-Pb isotopic ratios. *Gondwana Res.*, 75, 218–238.

Mancinelli, P., Scisciani, V., Pauselli, C., Stampfli, G. M., Speranza, F., and Vasiljević, I. (2022). Back-arc underplating provided crustal accretion affecting topography and sedimentation in the Adria microplate. *Mar. Pet. Geol.*, 136, article no. 105470.

McDonough, W. F. and Frey, F. A. (1989). REE in upper mantle rocks. In Lipin, B. and McKay, G. R., editors, *Geochemistry and Mineralogy of Rare Earth Elements*, pages 99–145. Min. Soc. Am. Chelsea, Michigan.

McKenzie, D. P. and O'Nions, R. K. (1991). Partial melt distributions from inversion of rare earth element concentrations. *J. Petrol.*, 32, 1027–1091.

Mével, C. (1981). Occurrence of pumpellyite in hydrothermally altered basalts from Vema Fracture Zone (Mid-Atlantic Ridge). *Contrib. Mineral. Petrol.*, 76, 386–393.

Monjoie, P., Lapierre, H., Tashko, A., Mascle, G. H., Dechamp, A., Muceku, B., and Brunet, P. (2008). Nature and origin of the Triassic volcanism in Albania and Othrys: a key to understanding the Neotethys opening? *Bull. Soc. Géol. Fr.*, 179, 411–425.

Morimoto, N. (1988). Nomenclature of pyroxenes. *Schweiz. Miner. Petrog.*, 68, 95–111.

Neubauer, F., Liu, Y., Cao, S., and Yuan, S. (2019). What is the Austroalpine mega-unit and what are the potential relations to Paleotethys Ocean remnants of southeastern Europe? *Geol. Carpath.*, 70, 16–20.

Nimis, P. (1999). Clinopyroxene geobarometry of magmatic rocks. Part 2: Structural geobarometers for basic to acid, tholeiitic and mildly alkaline magmatic systems. *Contrib. Mineral. Petrol.*, 135, 62–74.

Nimis, P. and Ulmer, P. (1998). Clinopyroxene geobarometry of magmatic rocks. Part 1: an expanded structuralgeobarometer for anhydrous and

hydrous, basic and ultrabasic systems. *Contrib. Mineral. Petrol.*, 133, 122–135.

Obenholzner, J. H. (1991). Triassic volcanogenic sediments from the Southern Alps (Italy, Austria, Yugoslavia)—a contribution to the "Pietra verde" problem. *Sediment. Geol.*, 74, 147–171.

Palinkaš, L. A., Borojević Šoštarić, S., Strmić Palinkaš, S., Crnjaković, M., Neubauer, F., Molnar, F., and Bermanec, V. (2010). Volcanoes in the Adriatic Sea: Permo-Triassic magmatism on the Adriatic-Dinaridic carbonate platform. *Acta Mineral. Petrograph.*, 8, 1–15.

Pamić, J. (1982). Correlation between Mesozoic spilite-keratophyre association of continental and oceanic origin as exemplified by the Dinarides. *Earth Evol. Sci.*, 2, 36–40.

Pamić, J. (1984). Triassic magmatism of the Dinarides in Yugoslavia. *Tectonophysics*, 109, 273–307.

Pamić, J. and Balen, D. (2005). Interaction between permo-Triassic rifting, magmatism and initiation of the Adriatic-Dinaridic carbonate platform (ADCP). *Acta Geol. Hung.*, 48, 181–204.

Pamić, J., Gušić, I., and Jelaska, V. (1998). Geodynamic evolution of the Central Dinarides. *Tectonophysics*, 297, 251–268.

Passglia, E. and Gottardi, G. (1973). Crystal chemistry and nomenclature of pumpellyites and jugoldites. *Can. Mineral.*, 12, 219–223.

Pe-Piper, G. (1998). The nature of Triassic extension-related magmatism in Greece: Evidence from Nd and Pb isotope geochemistry. *Geol. Mag.*, 135, 331–348.

Pe-Piper, G. and Mavronichi, M. (1990). Petrology, geochemistry and regional significance of the Triassic volcanic rocks of the Western Parnassos isopic zone of Greece. *Ofioliti*, 15, 269–285.

Pe-Piper, G. and Panagos, A. G. (1989). Geochemical characteristics of the Triassic Volcanic rocks of Evia: Petrogenetic and tectonic Implications. *Ofioliti*, 14, 33–50.

Pearce, J. A. (1982). Trace element characteristics of lavas from destructive plate boundaries. In Thorpe, R., editor, *Andesites*, pages 525–548. Wiley, New York.

Pearce, J. A. (1983). Role of the sub-continental lithosphere in magma genesis at active continental margins. In Hawkesworth, C. J. and Norry, M. J., editors, *Continental Basalts and Mantle Xenoliths*, pages 230–249. Shiva, Nantwich UK.

Pearce, J. A., Lippard, S. J., and Roberts, S. (1984). Characteristics and tectonic significance of supra-subduction zone ophiolites. In Kokelaar, B. P. and Howells, M. F., editor, *Marginal Basin. Geology*, volume 16, pages 17–94. Geol. Soc. Spec. Publ.

Philip, J., Masse, J.-P., and Camoin, G. (1995). Tethyan Carbonate Platforms. In Nairn, A. E. M., Ricov, L. E., Vrielynck, B., and Dércourt, J., editors, *The Ocean Basins and Margins*, volume 8, pages 239–265. Plenum Press, New York.

Plank, T. (2005). Constraints from Th/La on sediment recycling at subduction zones and the evolution of the continents. *J. Petrol.*, 46, 921–944.

Plank, T. and Langmiur, C. H. (1998). The chemical composition of subducting sediment and its consequences for the crust and mantle. *Chem. Geol.*, 145, 325–394.

Polat, A. and Hofmann, A. W. (2003). Alteration and geochemical patterns in the 3.7–3.8 Ga Isua greenstone belt, West Greenland. *Precambrian Res.*, 126, 197–218.

Polat, A., Hofmann, A. W., and Rosing, M. T. (2002). Boninite-like volcanic rocks in the 3.7–3.8 Ga Isua greenstone belt, West Greenland: geochemical evidence for intra-oceanic subduction zone processes in the early Earth. *Chem. Geol.*, 184, 231–254.

Pomonis, P., Tsikouras, V., and Hatzipanagiotou, K. (2004). Comparative geochemical study of the Triassic trachyandesites of Glykomilia and alkali basalts from the Koziakas ophiolite mélange (W. Thessaly): implications for their origin. *Bull. Geol. Soc. Greece*, 36, 587–596.

Pouchou, J. L. and Pichoir, F. (1985). "PAP" (φ-ρ-Z) correction procedure for improved quantitative microanalysis. In Armstrong, J. T., editor, *Microbeam Analysis*, pages 104–106. San Francisco Press, San Francisco.

Putirka, K. (2008). Thermometers and Barometers for Volcanic Systems. *Rev. Mineral. Geochem.*, 69, 61–120.

Rahn, M., Mullis, J., Erdelbrock, K., and Frey, M. (1994). Very low-grade metamorphism of the Taveyanne greywacke, Glarus Alps, Switzerland. *J. Metamorph. Geol.*, 12, 625–641.

Robertson, A. H. F. (2007). Overview of tectonic settings related to the rifting and opening of Mesozoic ocean basins in the Eastern Tethys: Oman, Himalayas and Eastern Mediterranean regions. *Geol.*

Soc. Spec. Publ. London, 282, 325–389.

Saccani, E. (2015). A new method of discriminating different types of post-Archean ophiolitic basalts and their tectonic significance using Th-Nb and Ce-Dy-Yb systematics. *Geosci. Front.*, 6, 481–501.

Saccani, E., Dilek, Y., Marroni, M., and Pandolfi, L. (2015). Continental margin ophiolites of Neotethys: Remnants of Ancient Ocean–Continent Transition Zone (OCTZ) lithosphere and their geochemistry, mantle sources and melt evolution patterns. *Episodes*, 38, 230–249.

Ščavničar, B., Ščavničar, S., and Šušnjara, A. (1984). Volcanogenic-sedimentary Middle Triassic in the area of the Suvaja stream (Svilaja Mt., Outer Dinarides). Prirodosl. istraž. *Acta Geol.*, 14, 35–82. (in Croatian, with English abstract).

Schmid, S. M., Bernoulli, D., Fügenschuh, B., Matenco, L., Scheffer, S., Schuster, R., Tischler, M., and Ustaszewski, K. (2008). The Alpine-Carpathian-Dinaridic orogenic system: correlation and evolution of tectonic units. *Swiss J. Geosci.*, 101, 139–183.

Schmid, S. M., Fügensschuh, B., Kounov, A., et al. (2019). Tectonic units of the Alpine collision zone between Eastern Alps and western Turkey. *Gondwana Res.*, 78, 308–374.

Schmidt, M. W. (1992). Amphibole composition in tonalite as a function of pressure; an experimental calibration of the Al-in-hornblende barometer. *Contrib. Mineral. Petrol.*, 110, 304–310.

Schweitzer, E. L., Papike, J. J., and Bence, A. E. (1979). Statistical analysis of clinopyroxenes from deep sea basalts. *Am. Mineral.*, 64, 501–513.

Scotese, C. R. (2002). 3D paleogeographic and plate tectonic reconstructions: The PALEOMAP. *Bull. Houston Geol. Soc.*, 44(9), 13–15.

Šegvić, B., Kukoč, D., Dragičević, I., Vranjković, A., Brčić, V., Goričan, Š., Babajić, E., and Hrvatović, H. (2014). New record of Middle Jurassic radiolarians and evidence of Neotethyan dynamics documented in a mélange from the Central Dinaridic Ophiolite Belt (CDOB, NE Bosnia and Herzegovina). *Ofioliti*, 39, 33–43.

Šegvić, B., Slovenec, D., Altherr, R., Babajić, E., Ferreiro Mählmann, R., and Lugović, B. (2019). Petrogenesis of high-grade metamorphic soles from the Central Dinaric Ophiolite belt and their significance for the Neotethyan evolution in the Dinarides. *Ofioliti*, 44, 1–30.

Šegvić, B., Slovenec, D., and Badurina, L. (2022). Major and rare earth element mineral chemistry of low-grade assemblages inform dynamics of hydrothermal ocean-floor metamorphism in the Dinaridic Neotethys. *Geol. Mag.*, pages 1–27.

Šegvić, B., Slovenec, D., Schuster, R., Babajić, E., Badurina, L., and Lugović, B. (2020). Sm-Nd geochronology and petrologic investigation of a sub-ophiolite metamorphic sole from the Dinarides (Krivaja-konjuh ophiolite complex, Bosnia and Herzegovina). *Geol. Croat.*, 73, 1–11.

Singh, A. K., Khogenkumar, S., Singh, L. R., Bikramaditya, R., Khuman, C. M., and Thakur, S. (2016). Evidence of Mid-ocean ridge and shallow subduction forearc magmatism in the Nagaland-Manipur ophiolites, northeast India: constraints from mineralogy and geochemistry of gabbros and associated mafic dykes. *Chem. Erde-Geochem.*, 76, 605–620.

Slovenec, D., Lugović, B., Meyer, H.-P., and Garapić-Šiftar, G. (2011). A tectono-magmatic correlation of basaltic rocks from ophiolite mélanges at the north-eastern tip of the Sava-Vardar suture Zone, Northern Croatia, constrained by geochemistry and petrology. *Ofioliti*, 36, 77–100.

Slovenec, D., Lugović, B., and Vlahović, I. (2010). Geochemistry, petrology and tectonomagmatic significance of basaltic rocks from the ophiolite mélange at the NW External-Internal Dinarides junction (Croatia). *Geol. Carpath.*, 61, 273–294.

Slovenec, D. and Šegvić, B. (2021). Middle Triassic high-K calc-alkaline effusive and pyroclastic rocks from the Zagorje-Mid-Transdanubian Zone (Mt. Kuna Gora; NW Croatia): mineralogy, petrology, geochemistry and tectono-magmatic affinity. *Geol. Acta*, 19, 1–23.

Slovenec, D., Šegvić, B., Halamić, J., Goričan, Š., and Zanoni, G. (2020). An ensialic volcanic arc along the northwestern edge of Palaeotethys-Insights from the Mid-Triassic volcanosedimentary succession of Ivanščica Mt. (northwestern Croatia). *Geol. J.*, 55, 4324–4351.

Smirčić, D. (2017). *Genesis of Middle Triassic volcaniclastic deposits in the External Dinarides*. PhD thesis, Zagreb University. 217 p. (in Croatian, with English summary).

Smirčić, D., Aljinović, D., Barudžija, U., and Kolar-Jurkovšek, T. (2020). Middle Triassic syntectonic

sedimentation and volcanic influence in the central part of the External Dinarides, Croatia (Velebit Mts). *Geol. Q.*, 64, 220–239.

Smirčić, D., Kolar-Jurkovšek, T., Aljinović, D., Barudžija, U., Jurkovšek, B., and Hrvatović, H. (2018). Stratigraphic definition and correlation of the Middle Triassic volcaniclastic facies in the External Dinarides: Croatia and Bosnia and Herzegovina. *J. Earth Sci.*, 29, 864–878.

Smith, E. I., Sánchez, A., Walker, J. D., and Wang, K. (1999). Geochemistry of mafic magmas in the Hurricane Volcanic Field, Utah: implications for small- and large scale chemical variability of the lithospheric mantle. *J. Geol.*, 107, 433–448.

Stampfli, C., Hochard, C., Vérard, C., Wilhem, J., and Von Raumer, J. F. (2013). The formation of Pangea. *Tectonophysics*, 593, 1–19.

Stampfli, G. M. and Borel, G. (2003). A revised plate tectonic model for the Western Tethys from Paleozoic to Cretaceous. In *AAPG International Conference*, pages 1–6. Barcelona, Spain.

Stampfli, G. M. and Borel, G. D. (2002). A plate tectonic model for the Paleozoic and Mesozoic constrained by dinamic plate boundaries and restored synthetic ocean isochrons. *Earth Planet. Sci. Lett.*, 196, 17–33.

Stampfli, G. M. and Borel, G. D. (2004). The TRANSMED transects in space and time: Constraints on the paleotectonic evolution of the Mediterranean domain. In Cavazza, W., Roure, F., Spakman, W., Stampfli, G. M., and Ziegler, P. A., editors, *The TRANSMED Atlas: the Mediterranean Region from Crust to Mantle*, pages 53–80. Springer-Verlag, Berlin.

Stampfli, G. M. and Hochard, C. (2009). Plate tectonics of the Alpine realm. *Geol. Soc. Spec. Publ. London*, 327, 89–111.

Sun, S. C., Zhang, L., Li, R. H., Hao, T. W., Wang, J. Y., Li, Z. Q., Zhang, F., Zhang, X. J., and Guo, H. (2019). Process and Mechanism of Gold Mineralization at the Zhengchong Gold Deposit, Jiangnan Orogenic Belt: Evidence from the Arsenopyrite and Chlorite Mineral Thermometers. *Minerals*, 9, article no. 133.

Sun, S. S. and McDonough, W. F. (1989). Chemical and isotopic systematics of oceanic basalts: implications for mantle composition and processes. In Saunders, A. D. and Norry, M. J., editors, *Magmatism in Ocean Basins*, volume 42, pages 313–345. Geol. Soc. Spec. Publ., London.

Šušnjara, A., Sakač, K., Gabrić, A., and Jelen, M. (1992). Upper Permian evaporites and associated rocks of Dalmatia and bordeline area of Lika and Bosnia. *Geol. Croat.*, 45, 95–114.

Swinden, H. S., Jenner, G. A., Fryer, B. J., Hertogen, J., and Roddick, J. C. (1990). Petrogenesis and paleotectonic history of the Wild Bight Group, an Ordovician rifted island arc in central Newfoundland. *Contrib. Mineral. Petrol.*, 105, 219–241.

Taylor, S. R. and McLennan, S. M. (1985). *The Continental Crust: Its Composition and Evolution*. Blackwell Scientific Publication, Oxford.

Trubelja, F., Burgath, K. P., and Marchig, V. (2004). Triassic magmatism in the area of the Central Dinarides (Bosnia and Herzegovina): Geochemical Resolving of tectonic setting. *Geol. Croat.*, 57, 159–170.

van Hinsbergen, D. J. J., Hafkenscheid, E., Spakman, W., Meulenkamp, J. E., and Wortel, R. (2005). Nappe stacking resulting from subduction of oceanic and continental lithosphere below Greece. *Geology*, 33, 325–328.

van Hinsbergen, D. J. J. and Schouten, T. L. A. (2021). Deciphering paleogeography from orogenic architecture: constructing orogens in a future supercontinent as thought experiment. *Am. J. Sci.*, 321, 955–1031.

van Hinsbergen, D. J. J., Torsvik, T., Schmid, S. M., Matenco, L., Maffione, M., Vissers, R. L. M., Gürer, D., and Spakman, W. (2020). Orogenic architecture of the Mediterranean region and kinematic reconstruction of its tectonic evolution since the Triassic. *Gondwana Res.*, 81, 79–229.

Velledits, F. (2004). Anisian terrestrial sediments in the Bükk Mountains (NE Hungary) and their role in the Triassic rifting of the Vadar-Meliata branch of Neo-Tethys ocean. *Riv. Ital. Paleontol. S.*, 110, 659–679.

Velledits, F. (2006). Evolution of Bükk Mountains (NE Hungary) during the Middle-Late Triassic asymmetric rifting of the Vadar-Meliata branch of the Neotethys Ocean. *Int. J. Earth Sci.*, 95, 395–412.

Vishnevskaya, V. S., Djerić, N., and Zakariadze, G. S. (2009). New data on Mesozoic radiolaria of Serbia and Bosnia, and implications for the age and evolution of oceanic volcanic rocks in the Central and Northern Balkans. *Lithos*, 108, 72–105.

Vlahović, I., Mandić, O., Mrinjek, E., Bergant, S.,

Ćosović, V., De Leeuw, A., Enos, P., Hrvatović, H., Matičec, D., Mikša, G., Nemec, W., Pavelić, D., Pencinger, V., Velić, I., and Vranjković, A. (2012). Marine to continental depositional systems of Outer Dinarides foreland and intra-montane basins (Eocene-Miocene, Croatia and Bosnia and Herzegovina). *J. Alp. Geol.*, 54, 405–470.

Vlahović, I., Tišljar, J., Velić, I., and Matičec, D. (2005). Evolution of the Adriatic Carbonate Platform: Paleogeography, main events and depositional dynamics. *Palaeogeogr. Palaeoclimatol. Palaeoecol.*, 220, 333–360.

Walter, M. J. (1998). Melting of garnet peridotite and the origin of komatiite and depleted lithosphere. *J. Petrol.*, 39, 29–60.

Wang, X.-C., Xu, B., Wilde, S. A., and Pang, C. J. (2016). Origin of arc-like continental basalts: Implications for deep-Earth fluid cycling and tectonic discrimination. *Lithos*, 261, 5–45.

Weis, D., Kieffer, B., Maerschalk, C., Barling, J., de Jong, J., Williams, G. A., Hanano, D., Pretorius, W., Mattielli, N., Scoates, J. S., Goolaerts, A., Friedman, R. M., and Mahoney, J. B. (2006). High-precision isotopic characterization of USGS reference materials by TIMS and MC-ICP-MS. *Geochemistry Geophys. Geosystems*, 7, article no. 2006GC001283.

Whitney, D. L. and Evans, B. W. (2010). Abbreviations for names of rock-forming minerals. *Am. Mineral.*, 95, 185–187.

Wilson, M. (1989). *Igneous Petrogenesis*. Unwin Hyman Ltd., London.

Winchester, J. A. and Floyd, P. A. (1977). Geochemical discrimination of different magma series and their differentiation products using immobile elements. *Chem. Geol.*, 20, 325–343.

Wood, B. J. (2004). Melting of fertile peridotite with variable amounts of H_2O. *Geophys. Monogr. Ser.*, 150, 69–80.

Wood, D. A. (1980). The application of a Th-Hf-Ta diagram to problems of tectonomagmatic classification and establishing the nature of crustal contamination of basaltic lavas of the British Tertiary volcanic province. *Earth Planet. Sci. Lett.*, 50, 11–30.

Workman, R. K. and Hart, S. R. (2005). Major and trace element composition of the depleted MORB mantle (DMM). *Earth Planet. Sci. Lett.*, 231, 53–72.

Xie, Q., Kerrich, R., and Fan, J. (1993). HFSE/REE fractionations recorded in three komatiite-basalt sequences, Archean Abitibi greenstone belt: Implications for multiple plume sources and depths. *Geochim. Cosmochim. Acta*, 57, 4111–4118.

Zane, A. and Weiss, Z. A. (1998). Procedure for classifying rock-forming chlorites based on microprobe data. *Rend. Lincei*, 9, 51–56.